www.lpr-journal.org

# LASER & PHOTONICS REVIEWS

WILEY-VCH

REPRINT

LASER
& PHOTONICS
REVIEWS

Laser Photonics Rev. **8,** No. 5, 687–715 (2014) / **DOI** 10.1002/lpor.201300222

**Abstract** Because of long-range order and high chemical purity, organic crystals have exhibit unique properties and attracted a lot of interest for application in solid-state lasers. As optical gain materials, they exhibit high stimulated emission cross section and broad tunable wavelength emission as similar to their amorphous counterpart; moreover, high purity and high order give them superior properties such as low scattering trap densities, high thermal stability, as well as highly polarized emission. As electronic materials, they are potentially able to support high current densities, thus making it possible to realize current driven lasers. This paper mainly describes recent research progress in organic semiconductor laser crystals. The building molecules, crystal growth methods, as well as their stimulated emission characteristics related with crystal structures are introduced; in addition, the current state-of-the-art in the field of crystal laser devices is reviewed. Furthermore, recent advances of crystal lasers at the nanoscale and single crystal light-emitting transistors (LETs) are presented. Finally, an outlook and personal view is provided on the further developments of laser crystals and their applications.

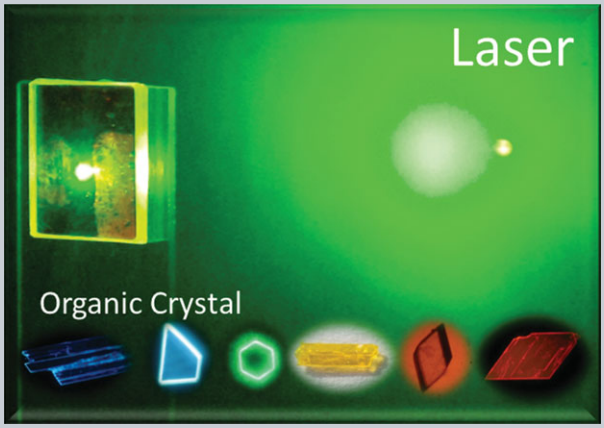


REVIEW ARTICLE

# Functional organic single crystals for solid-state laser applications

**Hong-Hua Fang[1], Jie Yang[1,4], Jing Feng[1], Takeshi Yamao[2], Shu Hotta[2], and Hong-Bo Sun[1,3,*]**

## 1. Introduction

Nowadays, as in the past, inorganic semiconductor crystal materials play fundamental roles in modern laser physics, nonlinear optics and quantum electronics. Understanding and ingenious utilization of these active crystals have led to a veritable revolution in the progress of solid-state laser engineering and photonic technology. In recent years, organic crystals based on $\pi$-conjugated semiconductor molecules have captured more and more interest as active building materials for photonic applications [1]. They are not only promising for economic reasons, but also for the strikingly different optoelectronic properties from those of their inorganic counterparts as well as much more flexibility and diversity in material design. They offer the possibility of tuning their properties by "chemical tailoring", i.e., by modifying molecular backbone structures and by varying substituents, which can modify the molecular packing and thereby incorporate novel functionalities.

Organic molecules have gained attention for laser applications as early as in 1961 [2], only one year after the invention of the first laser. Dye lasers were independently realized by P. P. Sorokin and F. P. Schäfer (and colleagues) in 1966 [3]. Soon after, dye-doped matrix laser were introduced in 1967 by Soffer and McFarland [4]. Stimulated emission (SE) was observed in doped single crystals in 1972 [5, 6]. In 1990s, lasing in conjugated polymer thin films was demonstrated [7–13]. Since then, the concept of organic semiconductor solid-state lasers became a hot topic [14–16], and huge number of organic semiconductor laser materials have been developed. Based on structural considerations, organic semiconductor laser media are primarily composed of three main categories: small molecule amorphous films, polymers and organic crystals. Progress on small molecule and polymer lasers has been well documented in many excellent reviews [14, 15, 17–22]. For brevity, they are not included here.

Organic semiconductor crystals are materials in which small size conjugated molecules are held together with long-range order via weak non-bonding interactions, such as van der Waals forces. Because of relative weak intermolecular interaction, electronic charge overlap between molecules is weak, and therefore the constituent molecules retain their identity to some extent. This is in contrast to

[1] State Key Laboratory on Integrated Optoelectronics, College of Electronic Science and Engineering, Jilin University, 2699 Qianjin Street, Changchun 130012, China
[2] Department of Macromolecular Science and Engineering, Graduate School of Science and Technology, Kyoto Institute of Technology, Matsugasaki, Sakyo-ku, Kyoto 606–8585, Japan
[3] College of Physics, Jilin University, 119 Jiefang Road, Changchun 130023, China
[4] Zernike Institute for Advanced Materials, University of Groningen, Nijenborgh 4, Groningen 9747 AG, The Netherlands
*Corresponding author: e-mail: hbsun@jlu.edu.cn

the inorganic counterpart, where the individual properties of constituent particles in the crystal are completely lost. However, the intermolecular electronic coupling in organic crystals cannot be ignored; the molecular packing would affect the $\pi$-orbital overlap in crystal, therefore resulting in different electronic and optical properties in crystals. To increase overlap between $\pi$-orbitals of neighboring molecules can cause delocalization of the polarons/excitons, leading to increase of charge carrier mobility [23]. It is well recognized that the organic single crystals exhibit superior charge–carrier transport properties over their amorphous counterparts, as their charge carrier mobility in pure organic crystals is 3 – 4 orders enhanced. The state-of-the-art of mobility reported in crystal is now in or even in excess of the range of that in amorphous silicon (1–10 $cm^2V^{-1}S^{-1}$) [24–26]. For example, the intrinsic hole mobility in p-type single crystal rubrene OFETs can reach up to 20 $cm^2V^{-1}S^{-1}$ [27]. High mobility is helpful for the realization of high injection current density, which is essential for realizing electrically pumped lasers. T. Takenobu has recently reported that hundreds A/$cm^2$ current density can be realized without degradation of external electroluminescence quantum efficiency in single-crystal [28]; K. Sawabe further escalated current densities up to 10 kA/$cm^2$ [29]. On the other hand, the crystals have numerous advantages in optical properties, such as highly polarized emission [30–33], selfwaveguide propagation [34, 35] and high refractive indices [36–38], which are relevant to the ordered molecular arrangement. Moreover, clean cleaved facets can be obtained thanks to their well-defined crystalline structure, thus forming self-laser-cavity. In the organic crystals, the optoelectronic properties depend on intermolecular contributions thus vary significantly on molecular packing and the resultant intermolecular electronic coupling. It offers a great opportunity to design and incorporate novel properties in crystals in a desired way through properly selecting the substituent pattern. In addition, the crystals allow a maximum possible packing density and best thermal and photochemical stability among the organic materials [39]. Because of these significant advantages, organic crystals have been considered as promising candidates for optoelectronic applications.

In recent years, especially in the last decade, organic crystals have played an important role in the development of organic semiconductor lasers. Various crystals combined with high luminescence efficiency and high carrier mobility have been developed. Great efforts have been performed towards cheap and high performance laser devices. In this paper, we would like to review the latest progress of organic laser crystals, emphasizing on their unique properties and lasing oscillation from different resonators. This paper is structured as follows: in Sec. 2, we will briefly introduce the building molecules, crystal growth methods along with their characteristics and advantages. Section 3 will be devoted to the overview of crystal structures, amplified spontaneous emission, and two-photon excited upconversion lasing. In the next section, different laser structures along with corresponding fabrication technologies, as well as lasing properties are presented. In Sec. 5, the status of research on the single crystal light-emitting transistors (LETs) towards current-driven laser is discussed. The final section includes the issues and outlook for future research in this field.

## 2. Building materials and growth technique for laser crystals

### *2.1. Building molecules*

#### 2.1.1. From molecules to molecular assemblies

When the individual molecules self-assemble into aggregates, the absorption and emission properties of molecules can change dramatically, which are often associated with specific intermolecular interactions [40–43]. These are preformed by the steric and electronic requirements of the molecules. Exciton effects are extensively observed in molecular aggregates, which induces spectral shifts or band splitting (Davydov splitting), and have been explained in terms of molecular exciton coupling theory [44], i.e., coupling of transition moments of the constituent molecules. The excitonic interaction depends on coulombic interactions of the spatial distribution of the transition dipole densities and thus sensitive to the relative positions of the molecules to their neighbors. Depending on the orientation of the molecular transition dipole moments, the molecular aggregates may exhibit hypsochromically shifted H-bands or bathrochromically shifted J-bands in their absorption spectrum, forming so-called H-type or J-type aggregates. Details of the spectral signatures have been intensively investigated by Spano et al. over the last decade [45–49].

In H-aggregates, the molecular transition dipole moments are antiparallel to each other, so that their sum cancels out at the lowest excited states. Thus, their lowest optical transitions are forbidden, while the higher ones are allowed. As a result, the transition from the excited state to the ground state is very fast, thus the main absorption peak shifts to higher energies and fluorescence is quenched in comparison to the single molecule. It is important to note that this does not necessarily imply low photoluminescence (PL) quantum yields in H-aggregate samples. Highly emissive H-aggregate have been reported in many single crystals [50–52]. J-aggregates on the other hand, dominated by "head-to-tail" orientations, and are characterized by little Stokes-shifted fluorescence that has a high quantum yield. The lowest lying exciton state has enhanced oscillator strength that gives rise to increased rate of spontaneous emission compared to that of the monomer and can be good candidate to show optical "superradiance".

The superradiance was theoretically predicted by Dicke [53], who described that when a macroscopic number of two-level dipoles were placed in a small volume, coherent coupling between dipoles develops by means of photon exchange, which results in cooperative recombination. Thus it can be applied for coherent electromagnetic pulse generation [54] or superradiant echo [55]. The superradiance is due to the collective nature of the excited states on the aggregate, with a characteristic emission of a macroscopic

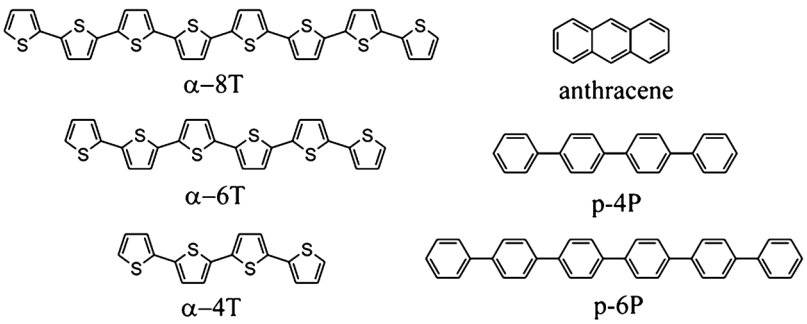


**Scheme 1** Crystal building constitutes. Molecular structures of typical conjugated all $\alpha$-linked oligophenylenes, $\alpha$-quaterthiophene ($\alpha$-4T), $\alpha$-sexithiophene ($\alpha$-6T) and $\alpha$-octithiophene ($\alpha$-8T); oligophenylenes, para-quaterphenylene (p-4P), para-sexiphenyl (p-6P); and anthracene.

optical polarization proportional to the number of correlated emitters ($N_c$), and therefore, the emitted intensity goes as ${N_c}^2$. As a consequence, the optical transition oscillator strength is enhanced and the excitation radiate their energy $N_c$ times faster than for incoherent emission. In the past decades, much work has been done to investigate and interpret this phenomenon both theoretically and experimentally [56–63]. Excitonic superradiance have been observed in several systems. For instance, Lim et al. observed superradiance in tetracene (TCN) nanoaggregates with ps time-resolved spectroscopy, finding a short-lived superradiant exciton delocalized over ∼10 molecules [64], and, recently, in TCN single crystals by Camposeo et al. [62].

It is important to note that the intrinsic PL properties of crystals are usually masked by inner filter effects, such as self-absorption, which arises from their high optical density. Furthermore, PL characteristics can be strongly altered by the presence of trap, as introduced e.g. by contaminations and structural defects, which might be able to quench the bulk PL. Thus, in order to properly determine whether the exciton is J-type or H-type, the single crystals have to be carefully purified and optical thin samples should be used to minimize the inner filter effects. The computational work of F. C Spano shows that in H(J)-aggregates the ratio of the 0-0 to 0-1 emission intensities increases (decreases) with disorder and increases (decreases) with increasing temperature [48]. Thus, in addition to aforementioned method, a comparison of PL at different temperature and observation of the changes in the emission line shape and radiative rate is helpful for gauging aggregate types.

### 2.1.2. Molecules for laser crystals

The lasing performance of device is dependent on intrinsic gain response of active materials. For a good laser crystal, several prerequisites have to be fulfilled: 1) high singlet exciton radiation recombination efficiency (high intrinsic quantum yield and high radiative rates); 2) a four-level energy level structure (large stokes shift, fast vibrational relaxation within excited state and ground state); 3) small excited state absorption and singlet-singlet bimolecular annihilation. Net optical gain only realized when the optical losses are overcome by stimulated emission, and resulting in amplified spontaneous emission (ASE), which is characterized of spectrally narrowed emission with a threshold upon increasing the excitation. ASE occurs when the spontaneously emitted photons are amplified by stimulated emission (SE) process during waveguide propagation in gain medium. This is why it depends significantly on the morphology of materials and waveguide length [65]. Through the Variable Stripe Length (VSL) technique, the gain efficiency for different excitation intensities can be easily determined. It has become a popular way to characterize optical gain properties of laser materials. In 1997, Fichou et al. reported stimulated emission phenomena from monolithic organic single crystal of thiophene oligomers: $\alpha$-Octithiophene [66]. Since then, ASE have been confirmed in many organic crystals [67–76]. Up to now, several classes of molecular crystalline materials have been demonstrated to exhibit ASE phenomena, such as oligothiophenes [77–81], oligo(p-phenylene) [13, 35, 82, 83], thiophene/phenylene co-oligomers [33, 67, 68, 84–97], fluorene/phenylene co-oligomers [98], bis-Styrylbenzene derivatives [99–101], cyano derivatives [71, 73]. In this section, we will introduce some typical organic laser crystals.

$\alpha$-linked oligothiophenes, as classic materials for optoelectronic devices, play important role on the study of organic laser crystals. Stimulated emission (SE) was first observed in undoped $\alpha$-8T crystals (Scheme 1) [66]. The linear $\alpha$-8T molecules have quasi-planar all-trans conformation, and are all parallel to each other in crystal. If the excitation is high enough, electrons are pumped from the ground state to higher energy level. When the number of electron at excited state is larger than the ground state, population inversion is achieved. For $\alpha$-8T crystal, SE appears with narrow emission line initially peaking at 700 nm. When the pump energy is further increased, a second narrow line at 640 nm emerges. The two lines at 640 nm and 700 nm coincide with the two maxima of broad photoluminescence (PL). Similar phenomena have also been observed in $\alpha$-4T and $\alpha$-6T crystals [77, 102–105]. The SE lines correspond to transitions from the first ($S_1$) and second ($S_2$) vibrational excited state to the fundamental state $S_0$, as shown in Scheme 2 [66]. Un-substituted oligothiophenes ($\alpha$-nTs) generally have low luminescence efficiencies (less than 9 %), whose origin is probably related to strong intermolecular interactions. So recently, oligothiophenes with different functional group and fused thiophenes have been developed to weak the electronic interactions and to enhance the PL efficiency in solid state. For example, the functionalization of the

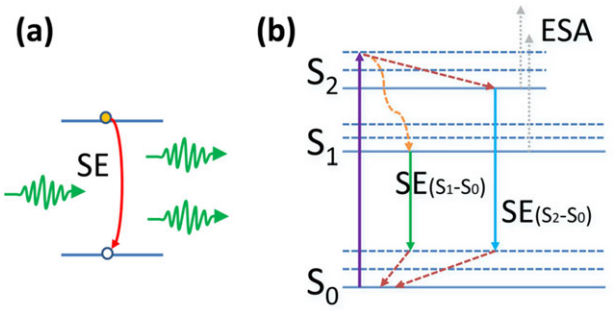


**Scheme 2** (a) Schematic illustation of he stimulated emission process. (b) Schematics of absorbing and emitting transitions in organic crystals along with relaxation processes. ESA: excited state absorption; SE($S_2$-$S_0$): stimulated emission from second vibrational level $S_2$ to ground state; SE($S_1$-$S_0$): stimulated emission from first vibrational level $S_1$ to ground state.

thienyl sulphur atom with two oxygens leads to solid state photoluminescence efficiencies of up to 37 %, and widely tunable PL emission [106].

Oligophenylenes are another well-documented class of molecular semiconductors, which exhibit high quantum yields of the emission in both solutions and solids [35, 70, 83, 107–111]. As model material, p-sexiphenyl (p-6P) crystals have been investigated extensively in self-waveguide and ASE properties [35, 107, 112]. Blue lasing is demonstrated in both close packed crystalline nanofiber films [83] and single selected p-6P nanofiber [113]. The nanofiber shows a high net gain of up to 103 $cm^{-1}$. It is should be stressed that the gain and lasing properties is strongly dependent on the experimental condition. For the same material, ASE behaves differently between under nanosecond and femtosecond pumping [70]. The result reported by Günter shows that excitation by femtosecond laser pulses leads to dual wavelength ASE at 427 and 450 nm in p-6P bulk crystals, while under nanosecond laser pulses excitation, there is only one peak at 450 nm. It suggests that the 427 nm emission may have larger nonradioactive losses at this transition. In fact, the ASE properties is significantly dependent on sample morphology. Adachi et al. reported that different peak wavelength of ASE in p-MSB crystal can be seen from crystals with different thickness [101]. When the thickness is less than 1 μm, ASE occurs mainly at $S_0$-$S_1$ transitions; when the thickness is larger than 2 μm, $S_0$-$S_2$ transitions dominate ASE spectrum. We have also observed similar results in BP2T crystal [114]. ASE firstly occurs at $S_0$-$S_2$ transitions for thick crystals. As further increasing the pump intensity, peak at $S_0$-$S_1$ transitions appears and dominates the spectrum eventually. The optical gain of the two transitions competing with each other. Actually, there is no intrinsic difference in photophysical parameters between the thin and thick crystals. However, inner filter effects, such as re-absorption process (related with crystal size), may affect their net gain properties.

Another class of materials with spectrally narrowed emissions are thiophene/phenylene co-oligomer (abbreviated as TPCOs), in which the thiophene and phenylene are hybridized at the molecular level. Over the past decade, a series of TPCOs have been developed, such as phenyl-capped oligothiophenes, block and alternating co-oligomer, thienyl-capped oligophenylenes [84, 115–119]. One of the advantages is that the extension of $\pi$-conjugation can be tuned as desired by changing the total ring number and their mutual arrangement of the thiophene and phenylene in the molecule, as shown in Scheme 3. For example, as a longer thiophene block is introduced to the oligomer with biphenyl groups at both ends, the HOMO–LUMO gap decreases in the order BP1T > BP2T > BP3T. ASE occurs at 466 nm for BP1T crystal [120], while the wavelength is shifted to 618 nm for BP3T [121]. ASE wavelength ranges from blue to red have been achieved in different TPCOs crystals [67, 68, 84, 85, 87, 89, 92, 93, 120, 122, 123]. Moreover, TPCOs have various molecular shapes, *e.g.* straight, bent, and zigzag, which is favorable for weakening intermolecular interaction and enhance photoluminescence emission. It is reported that the quantum yield of BP3T crystals is as high as 80 % [124]. Several crystals of such molecules display low threshold ASE at room temperature.

Poly(p-phenylene vinylene) derivatives (PPV) materials play a crucial role in the development of polymer laser. The first organic solid state laser was demonstrated in MEH-PPV [11]. Correspondingly, their oligomers compose one important class of building materials for laser crystals. Distyryl-benzene (DSB) is one of the simple and typical model compound for PPV, with a high PL quantum yield of ∼65% in crystal [125]. A number of distyryl-benzene derivates have been developed for understanding of structure–property relationships, as shown in Scheme 4. Ma's group, and Park et al. have developed several DSB-based materials with different substituents [99, 126–134]. Through proper molecular design, it is possible to tune the arrangement of molecule from one to another, hence obtaining high PL quantum yields. For example, the efficiency of CN-DPDSB is as high as 80% [71]. DBADCS crystals show efficient light amplification following different mechanisms (amplified spontaneous emission, multimode laser oscillations, and stimulated resonant Raman scattering; SRRS) [133].

Stimulated emission in organic crystals depends significantly on their quantum yield, but that's not the whole story. Other factors, such as excited-state absorption, internal conversion and Stokes shift in the crystal, have to be fulfilled. From the view of energy level, a four-energy system is favorable for population inversion. Most organic semiconductors form an approximate four level system via vibronic relaxation in the excited state. Park et al. have recently developed a novel class of crystals, hydroxy-substituted tetraphenyl imidazole (HPI) and its acetate-containing derivative, HPI-Ac (see Scheme 5) [135, 136]. Different from the common used oligomers, they are harnessed with a favorable four-level photophysical cycle based on excited-state intramolecular proton-transfer (ESIPT). The ESIPT molecules are normally more stable in E forms in the ground states but in K* forms in the excited

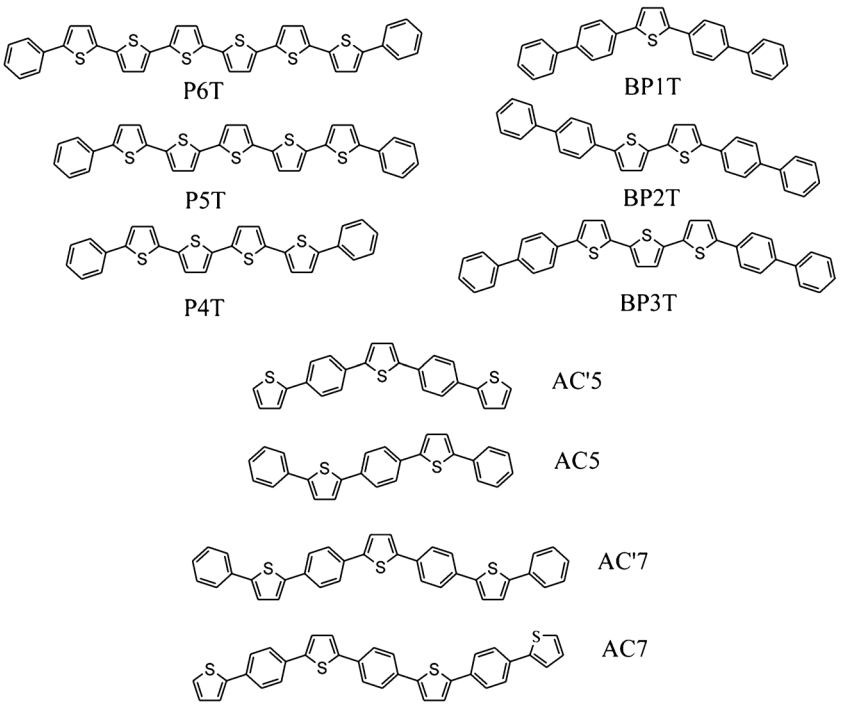


**Scheme 3** Various thiophene/phenylene co-oligomers (TPCOs).

states, photoexcitation of them is immediately followed by the four-level cyclic proton-transfer reactions (E-E*-K*-K-E) mediated by the intramolecular H-bonds (Scheme 5). Therefore, the absorption from E and emission from K* result in an abnormally large Stokes shift with no self-absorption. In these crystals, they demonstrated intense blue fluorescence and produced a straight path of blue ASE at a right angle to the photoexcitation, as shown in Fig. 1a.

Besides the diversity of building materials, one of the most amazing features is that the properties of organic crystals could be tailored and incorporated with additional

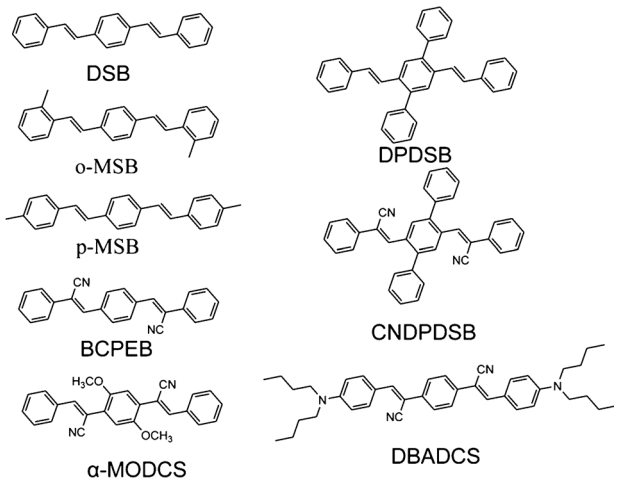


**Scheme 4** Molecular structures of bis-Styrylbenzene and their derivatives. 1,4-distyrylbenzene (DSB), 1,4-bis(2-methylstyryl) benzene (o-MSB), 1,4-bis(4-methylstyryl)benzene (p-MSB),1,4-bis(2-cyano-2-phenylethenyl)benzene (BCPEB), (a-MODCS), 2,5-diphenyl-1,4-distyrylbenzene (DPDSB), cyano substituted oligo(p-phenylene vinylene) (CNDPDSB), (2Z,2′Z)-2,2′-(1,4-phenylene)bis(3-(4-(dibutylamino)phenyl)acrylonitrile) (DBADCS).

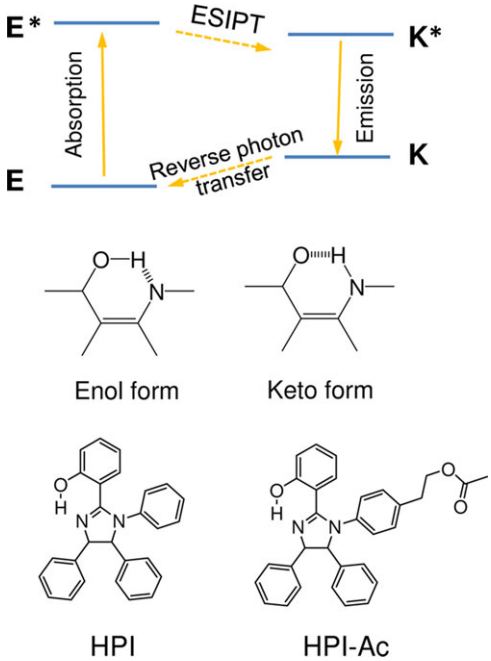


**Scheme 5** Schematic Representation of ESIPT Photocycle and molecule structure of HPI and HPI-AC. (Reproduced with permission [135]. Copyright 2005 American Chemical Society.)

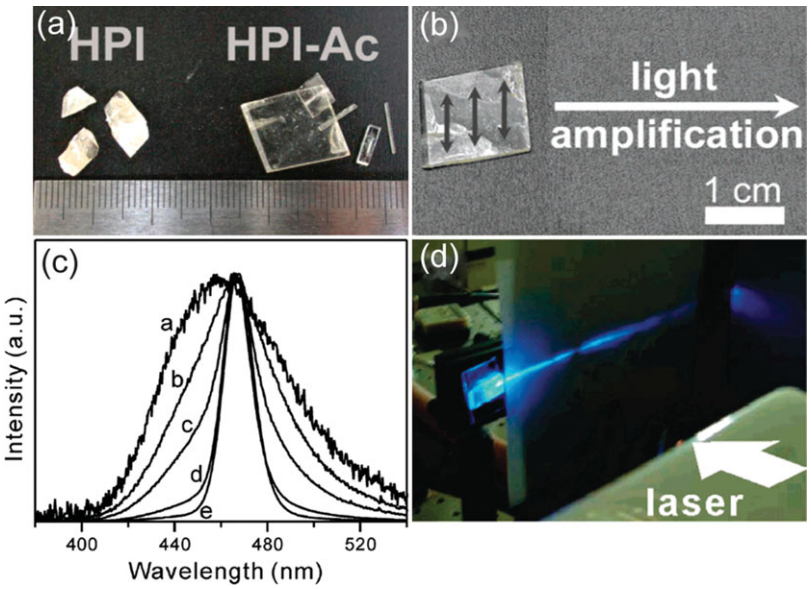


**Figure 1** (a) Photograph showing single crystals of HPI and HPI-Ac. (b) Schematic representation of the optimal polarization direction in the HPI-Ac single crystal. (c) Peak-normalized emission spectra of a single crystal of HPI-Ac at various pulse excitation energies: (d) Photograph of a straight path, at a right angle to the photoexcitation, of blue ASE at the excitation fluence of 10 mJ $cm^{-2}pulse^{-1}$. (Reproduced with permission [135]. Copyright 2005 American Chemical Society.)

functions. Organic materials that exhibit strong two-photon absorption and efficient two-photon fluorescence are attractive for applications such as data storage [137], optical limiting [138], single-crystal to single-crystal transformations [139], two-photon photopolymerization [140], fluorescence microscopy [141], and two-photon pumped (TPP) lasing [142]. TPP lasing are currently of considerable interest for upconversion lasers, as gain medium can be directly pumped at red or near-infrared wavelengths with relaxation of phase matching. Naturally, researchers did also think of the possibility of utilization with organic crystals, and achieved several successful examples. Sun's group has recently demonstrated amplified spontaneous emission from the single crystals of DBASDMB [143], Ph-TPA2 [144], cyano-substituted oligo(p-phenylenevinylene) crystals [32, 74] and crystals of 9,10-distyrylanthracene (DSA) derivatives [145]. Zhang and co-workers developed crystals of thiomethyl-terminated oligo(phenylene vinylene) for upconversion application [146]. Zhao et al. realized two-photon-pumped exciton polariton lasing in organic waveguiding nanostructures of 2-(N,N-diethylanilin-4-yl)-4,6-bis(3,5-dimethylpyrazol-1-yl)-1,3,5-triazine (DPBT) at 77 K [147]. Scheme 6 presents molecular structures of some reported crystals exhibited two-photon upconversion lasing properties. By utilizing two-photon absorption in organic crystal, it is possible to develop novel upconversion solid state lasers. This will be discussed in Sec. 4 in detail.

### *2.2. Growth of organic semiconductor single-crystals*

Lasing emission in organic crystals not only depends on internal factors, but also on the morphology and quality of crystals. For instance, defects would act as scattering centers and give rise to serious loss during light amplification. Therefore, crystals with fewer defects are preferred. Over past decades, a huge number of organic semiconductors

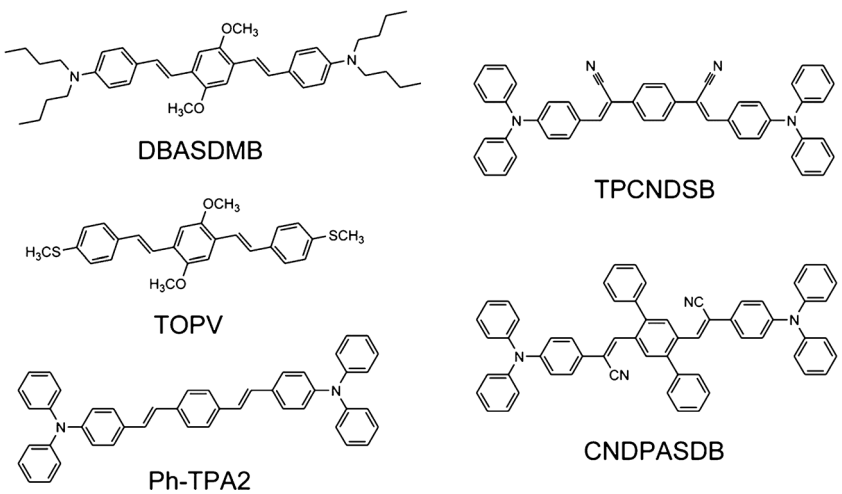


**Scheme 6** Molecule structures of organic crystals reported with efficient two-photon excited lasing properties. E,E-1,4-bis[4′-(N, N-dibutylamino)styryl]-2,5-dimethoxy-benzene (DBASDMB), thiomethyl-terminated oligo (phenylene vinylene)s with methoxyl side groups (TOPV), N-(4-{4-[4-(diphenylamino) styryl]styryl}phenyl)-N-phenylbenzene amine (Ph-TPA2), 1,4-bis[1-cyano-2-(4-(diphenylamino)phenyl)vinyl]-benzene (TPCNDSB), 1,4-bis(R-cyano-4-diphenylaminostyryl)-2,5-diphenylbenzene (CNDPASDB).

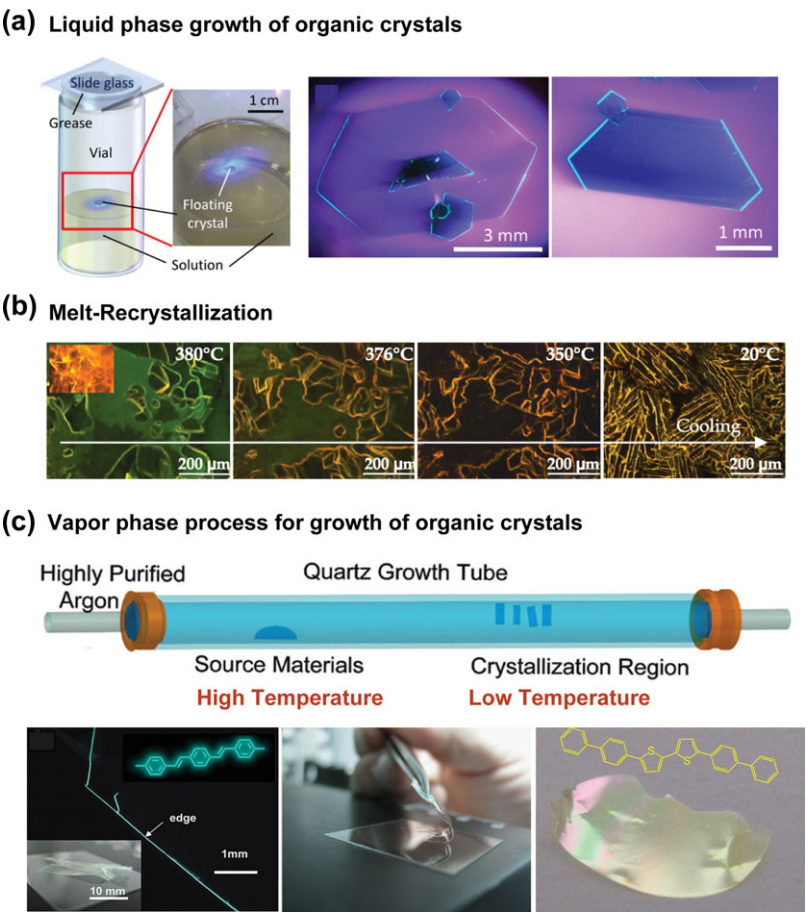


**Figure 2** Crystal growth methods: (a) Solution processes of organic crystals. (Reproduced with permission [157]. Copyright 2011 Elsevier B.V.) (b) Melt-recrystallization. (Reproduced with permission from [90]. Copyright 2010 American Chemical Society.) (c) Vapor process such as physical vapor transport technique. (Reproduced with permission from [173]. Copyright 2011 American Chemical Society.)

has been synthesized, but only a few have been crystallized into single crystals for physical property characterization and device construction. Compared with their inorganic counterparts, organic crystals have much lower melting point and sublimation temperature; therefore the crystal growth methods differ substantially from inorganic crystals [148]. In this section, we will give a brief introduction to organic crystal growth.

### 2.2.1. Crystallization from liquid phase

Perhaps the most simple and low-cost way to obtain single crystals is self-assemble in liquid phase. It is possible to get crystal in minutes by evaporating the solvent, adding poor solubility solvent or drop casting from organic solutions [149–155]. However, the crystal size is generally in nanoscale region. For some practical device applications, such as planar microcavity laser, scintillation detectors, large crystals of a few millimeters even centimeters are required. To get large crystal sizes from solution is a subtle and time consuming task, which may take several days, weeks, even months, depending on the type of materials. Crystallinity of organic semiconductors is dependent on intermolecular non-covalent interactions, such as hydrogen bonds and $\pi$-$\pi$ stacking interactions for molecular packing. The fastest crystal growth direction is along direction where the intermolecular interaction is strongest. In the case of elongated, needle-like crystals, the strong intermolecule interactions are maximized along with long axis. For platelet-like crystals, they generally have extensive network of interactions within XY plane [25]. Generally, crystallization is kinetically hindered and crystals grow only from supersaturated solutions [156]. There are several ways to archive this metastable state of supersaturation of solution. The easiest is increasing the concentration by evaporation of the solvent until crystallization sets in [153]. If solvent removal is not performed in a well-controlled way, it tends to produce many crystals in small size because of the spontaneous nucleation in a high-supersaturated solution.

Hotta et al. have recently developed constant-volume decreasing-temperature method to increase the size of crystal (as shown in Fig. 2a) [157]. In order to avoid spontaneous nucleation, they prepared a low-supersaturated solution. As the nuclei grow, the solution becomes less supersaturated and the driving force for the crystal growth decreases accordingly. To keep the crystal growth, the solution has to remain low supersaturated by adding source e.g., seed crystals or solute particulates. By applying this method, well-defined hexagon thiophene/phenylene co-oligomers (TPCOs) crystals (up to 7.6 $\times$ 4.4 mm, with thickness of 51 μm) have been successfully prepared. Yamao et al. have

developed a method to make the crystals grow directly on the substrate [158]. The growth apparatus is equipped with a radiator made of metal steel. The radiator can release the heat from the liquid to the atmosphere, then cool the substrate locally and keep the temperature lower than that of surrounding liquid. The crystals form directly on the substrate. This is convenient for further device fabrication.

In solution-based growth method, the solvent may intercalate or even incorporate into the crystal lattice during growth process. For this reason, the crystal lattice may be affected by solvent, and deviate significantly from the model of the perfect crystal; thereby adversely affecting the physical properties and device performance.

### 2.2.2. Melt-recrystallization

For liquid phase growth, organic semiconductors with good solubility in common solvents are required, which is not often the case and hence limits the application of this method. Melt growth techniques on the other hand do not have these restrictions, and one can generally prepare crystals in several hours. When the materials possess a well-defined melting point and high thermal stability at that temperature, it is possible to process materials by melt growth method. The most prominent advantage for this method is that it is possible to let the materials melt into the desired geometry for device applications. For example, Günter and coworkers melted the organic material and let it flow into predefined channels by capillary force, and crystallize there upon cooling. By this method, they have fabricated high-quality single-crystalline channel waveguides and integrated Mach-Zehnder modulators[159–161]. Various conjugated semiconducting oligomers, such as p-4P, anthracene, p-5P, p-6P, BP1T, AC5, TPB and TPP have been prepared by melt-growth method [90, 120]. However, when growth occurs in a small confined space; the crystals are apt to suffer from cracks and stresses caused by uneven thermal distribution or contact with the walls of the container. Figure 2b shows fluorescence image during the growth of a sample of TPP by the melting method. Crystalline domains are found in the case of the melted sample. The melt growth crystal often exhibit significantly broadened mosaicity due to formation of cracks and dislocations. The macroscopic order and the presence of cracks in this type of crystal are likely to be improved by adopting a slower and proper profile of temperature during the growth.

Another one important way is Czochralski method, which is frequently used for inorganic crystals [162]. In Czochralski method, a seed crystal is used in order to start growth. The melt materials crystallize on this seed, forming single crystal with the same orientation as the seed; therefore, it results in better-quality organic crystals. However, it has a small application range for organic materials; because high vapor pressure results in fast evaporation during the growth process. Only a few materials, which are inexpensive and available in large quantity, have been prepared by this method [148, 163].

### 2.2.3. Crystal growth from vapor phase

The most frequently used method for organic semiconductors single-crystal growth is the vapor growth technique. Most organic small molecules possess sufficient vapor pressure so that the vapor growth method can be efficiently used. For low solubility materials, physical vapor transport (PVT) proposed by Kloc and Laudise et al., is a very good selection [164, 165]. For instance, crystals of $\alpha$-hexathiophene ($\alpha$-6T), $\alpha$-octithiophene ($\alpha$-8T), $\alpha$-quaterthiophene ($\alpha$-4T), pentacene, anthracene and copper phthalocyanine have been prepared in horizontal or vertical PVT systems [166]. In this method, centimeter size crystals could be obtained in several hours.

Numerous modifications of PVT method have been developed by different research groups [68, 130, 167–171]. Although there are differences in apparatus, the basic principle of the physical vapor method is the same, as shown in Fig. 2c: the source material placed in the source tube of the reactor is heated at high temperature; then sublimated molecules are transported to a lower temperature zone and crystallize within a narrow temperature range. The vapor method allows both crystal growth and purification in a single process. For this reason, it is possible to grow crystal with high purity and high structural quality. Organic semiconductors and impurities are deposited in different locations because of different molecular weights. For better separation of the crystals from the impurities, the temperature gradient along the tube should be maintained sufficiently small (e.g., $\sim$5–10 $^{\circ}$C/cm). In addition, the inert gas can be used as a protector that prevents oxidation of the organic semiconductors. With optimized parameters, high quality crystals could be obtained. Recently, Chapman et al. have shown that single-crystals of rubrene can be grown to high-structural perfection, with rocking curve mosaic spreads as narrow as 0.0131$^{\circ}$ for the {100} and {001} planes for the best samples [172]. However, many other measured rubrene crystals possessed much broader mosaic with 0.15$^{\circ}$ Full width at half maximum (FWHM). The mechanism of forming such mosaic spreads in these crystals is unknown. Both the growth process and, more probably, carrier gas velocity, temperature gradient are responsible for defect formation in these crystals. In addition, molecular decomposition during the crystal growth process may further affect the crystal quality.

Nucleation control is required for the growth of a smaller number of nuclei into larger crystals without intergrowth. Sun et al. introduced adsorbent to control the degree of vapor saturation, the size and morphology of BSB-Me single crystals were significantly improved [173]. Adsorbents have proved to be indispensable in improving the quality of the as-fabricated BSB-Me crystals. In PVT, sublimation takes place at relatively high temperatures, so that there is a lot of energy in the system. The molecules have high enough kinetic energy to incorporate into the crystal lattice. With PVT, Ma and Sun et al. have prepared several kinds of doped organic crystals with high luminescent efficiency [174, 175]. Guest molecules could be doped uniformly in host molecule crystal lattice, as shown

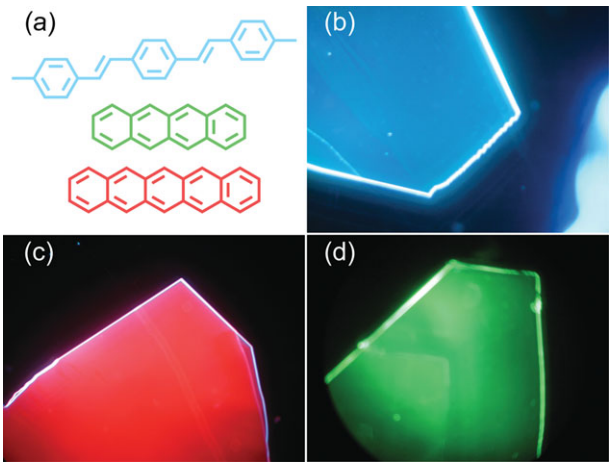


**Figure 3** Doped organic crystals. (a) The molecular structures of BSB-Me, tetracene, pentacene. (b) The pure BSB-Me crystal. (c) Pentacene doped BSB-Me crystal. (d) Tetracene-doped BSB-Me crystal photographs under the ultraviolet lamp. (Reproduced with permission [175]. Copyright 2012 Elsevier B.V.)

in Fig. 3. But the control of the doping concentration is not well understood.

Up to date, many organic crystals have been successfully prepared by the aforementioned method. However, the study on crystal quality, defect density, and grain boundaries in crystals grown by different methods is not enough. Clearly, the morphology and defect density is strongly depended on growth method. Conditions during the growth method also play important role. For example, growth of tetracene in Helium gas yields very thin and wide crystals, while slow growth in Argon gas yields much thicker and robust crystals [26, 176]. Another important factor is the purity of the starting materials. Empirically, different grades of material with same nominal purity might result in crystals of quite different quality. Furthermore, the role of defects on the optical and electronic properties in the organic crystals should be given more attention in future research.

## 3. Crystal structures and related optical properties

Oligomers, the crystal building molecules, typically have large aspect ratio (the length depends on the degree of oligomerization) [49, 89, 126, 177]. The molecular arrangements may be affected by the nature of the main chain, the presence or absence of side chains, and their nature (branched or linear) and their position of attachment (regioregularity) [178]. Single crystal structures with several molecules per unit cell (Z) are commonly observed in organic semiconductors, as shown in Fig. 4. It usually consists of one or two transnationally equivalent molecules. Take p-MSB for example (Fig. 4d), the crystals are characterized by the presence of the molecular layered structure in which the molecules form the well-known herringbone structure laterally spreading along the XY-plane [101]. In many crystals, the molecules are inclined against the molecular layer

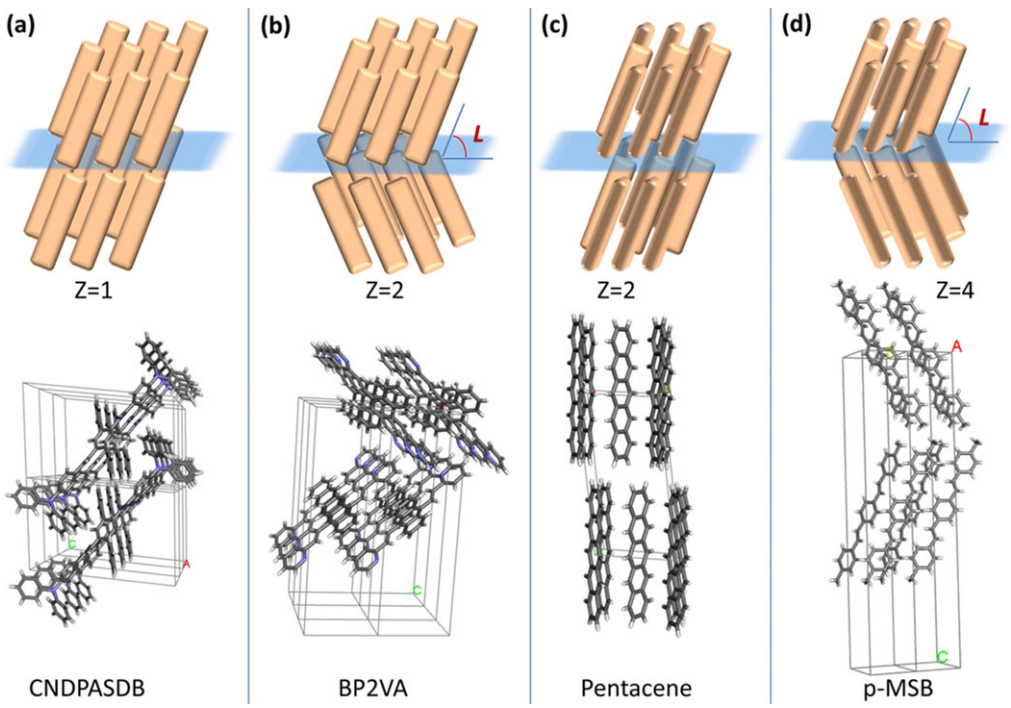


**Figure 4** Schematic of typical intermolecular arrangements in molecular crystals of conjugated oligomers, and molecular packing within the crystal structure of (a) 1,4-bis(R-cyano-4-diphenylaminostyryl)-2,5- diphenylbenzene (CNDPASDB), (b) 9,10-bis((E)-2-(pyrid-2-yl)vinyl)anthracene (BP2VA), (c) Pentacene, (d) 1,4-bis(4-methylstyryl)benzene (p-MSB).

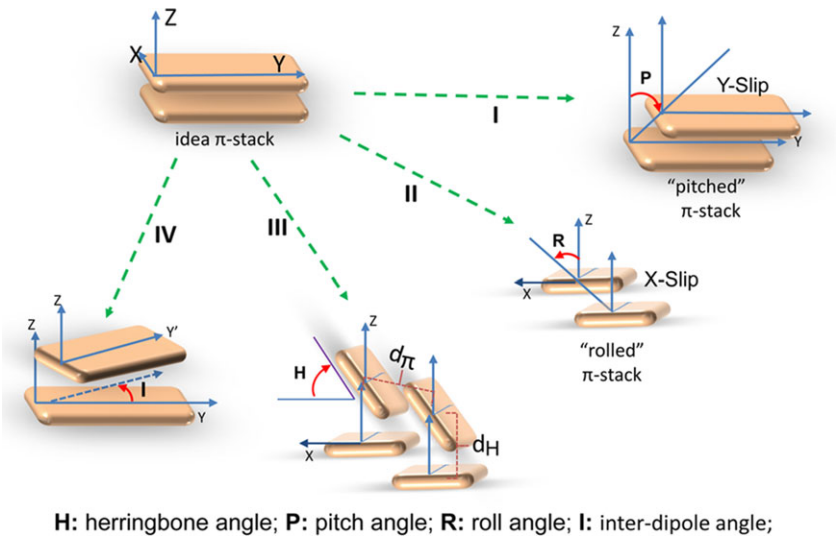


**Figure 5** Schematic of molecular arrangement in a crystal layer. (I) The translation of one molecule along the chain-axis direction, (II) the translation of one molecule along the in-plane transverse axis, (III) the rotation of one unit around its long axis, and (IV) the rotation of one molecule around the stacking axis while keeping the parallelism between the molecular planes.

plane because of intra-layer molecule interactions (usually much weaker than side-by-side interaction). The tilting can be measured by an angle between the molecular long axis and the normal to the bottom crystal plane. Depending on the nature of interaction between these two layer, it might form 'zig-zag' arrangement, thus double Z compared to single layer. The angle can be exactly 0° when the molecule and crystal are designed appropriately. This was done by Hotta et al. with BP1T-OMe, dimethoxy-capped BP1T (in this case, the crystals are orthorhombic with space group $Cmc2_1$) [179].

Within a single crystal layer, slipped face-to-face (or $\pi$-stack) arrangement is the simplest case. The inclinations may be described by two angles, which called "pitch" (P) and "roll" (R) in analogy with the nautical terms [178,180]. Figure 5 shows the definitions of the pitch (I) and roll (II) angles. When the molecular planes of adjacent stacks rotate around their long axis (See Fig. 5 III), edge-to-face herringbone arrangements are obtained. A typical example is Pentacene crystal (Fig. 4c), when viewed down the long molecular axis, the main chains appear to be stacked in a this pattern. With the increase of herringbone angle, the packing changed from face-to-face to herringbone motif, where the inversion point is $d_H < d\pi$ ($d_H$ is the nearest neighbor distance for herringbone, while $d\pi$ is the nearest distance for $\pi$-stacked neighbors) [181]. Another packing motif between two nearest molecules is cross-dipole arrangement (IV in Fig. 5).

As mentioned above, H-aggregation arrangements (with strong side-by-side interaction) often lead to serious declines in the optical properties because of considerable $\pi-\pi$ overlap. Through a proper alignment of the molecules in the crystal lattice, the optical properties of crystal can be essentially changed [182]. When the short axes are inclined to each other, hence minimization of $\pi-\pi$ overlap, it is possible to realize high photoluminescence in crystals for lasing application. The examples include DSB (65% quantum yield) and DSB with four methyl-substituents (quantum yield of 81%) [50, 183]. In 2001, Tang discovered unusual aggregation-induced emission (AIE) phenomenon [184]. Since then, the concept of AIE has been employed to design efficient fluorescent materials in the solid state, and a series of AIE molecules with highly twisted structures have been developed [185–187]. The twisted geometry of molecule weakens its intermolecular interaction and minimizes the likelihood of excimer formation in the crystal. This is helpful in achieving high quantum efficiency. Indeed, stimulated emissions have been observed from several AIE crystals [74]. Another distinctive strategy is to construct the cross stacking of transition dipoles (as shown in Fig. 5 IV), which is theoretically predicted that it ensures the optically allowed transition from the lowest excited state to the ground state. Therefore, it promote for efficient light emission. Ma et al. demonstrated the high fluorescence efficiency (80%) of such stacking modes in trans-DPDSB [99]. Tian et al. observed cross dipole packing with rotation angle of ca. 67° and 60% quantum efficiency in 9,10-bis (2,2-diphenylvinyl) anthracene (BDPVA) crystal [188].

### *3.1. Self-waveguided and highly polarized amplified spontaneous emission*

In relation to the molecular alignment, the crystals always exhibit well defined polarization of the electronic states, and strong optical anisotropy [31, 33, 37, 38]. For example, the probability of optical transitions relies on the crystal orientation with respect to polarization of the excitation light. In order to maximize light absorption, the polarization of pumping light beams should be precisely aligned by half-wavelength plate to couple to the molecular electronic transition moment in crystal. When the polarization of pump coincides with the direction of molecular transition, the absorption of pump light is the most effective. Consequently, less pump fluence is needed to reach the ASE threshold.

High ordered excitonic transition is responsible for the edge emission in the crystals, as shown in Fig. 6a–c. Strong emission occurred solely at the edges of crystals, while surface emission is nearly absent. In the TPCOs, the molecules

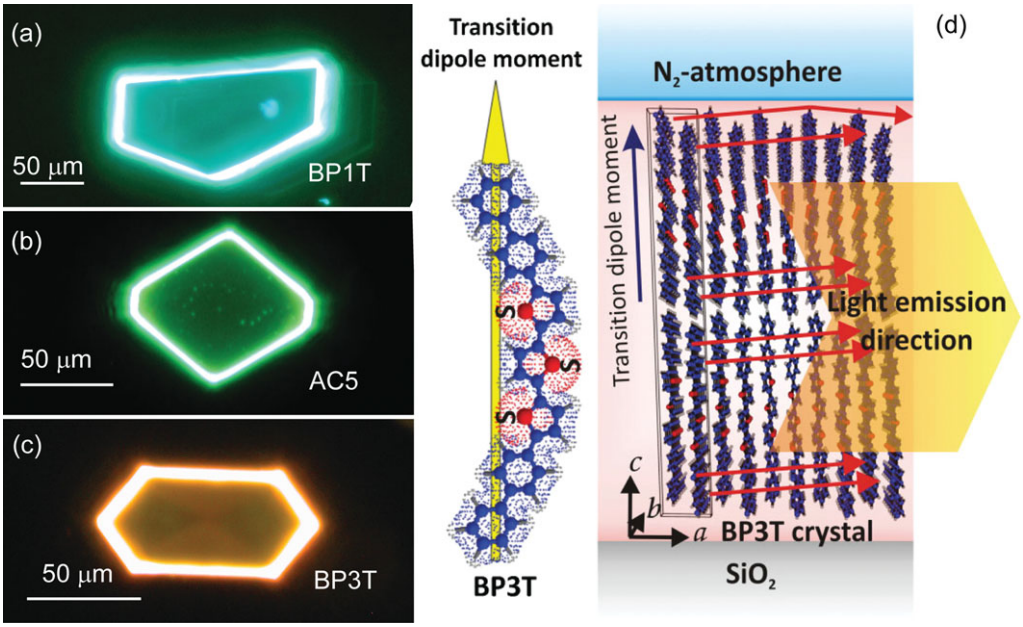


**Figure 6** (a)-(c) Photograph of BP1T, AC5, and BP3T crystal. (d) A schematic illustration of the self-waveguided edge-emission mechanisms, showing the BP3T molecules stacked nearly perpendicular to the crystal plane with their transition dipole moments and molecular long axis in parallel. (Reproduced with permission from [124]. Copyright 2009 WILEY-VCH Verlag GmbH & Co. KGaA, Weinheim.)

are arranged layer by layer, laterally spreading along the *XY*-plane. Because the transition dipoles are disposed vertical to the substrate plane, so the molecular light emission tends to emit parallel with the *XY*-plane, as shown in Fig. 6d. On the other hand, because of high refractive indexes of crystals, the TPCOs act as excellent waveguide, causing the light having a small grazing angle to be totally internally reflected between the surfaces. It further prevents emission from leaking out from the crystal surface, so that glassy emission is observed from the edge [189, 190].

Most of TPCOs crystals are shaped as thin platelets. It is controlled by the anisotropy of intermolecular interactions: the largest crystal dimension corresponds to the direction of the strongest interactions and, presumably, the strongest overlap of $\pi$-orbitals of adjacent molecules. In contrast to slab crystals, many of crystals are prone to grow into needle-like morphology [34, 152, 191], serving as active waveguide. Take Ph-TPA2 for example [144], blue-green emission emit at tips and relatively weaker emission are from the bodies, a typical characteristic of an optical waveguide behavior. Recently, Ma et al. reported tubular crystals of 1,4-bis(2-cyano-2-phenylethenyl)benzene (BCPEB) [192]. The hollow-like topological structure enables the crystal to exhibit optical waveguide emission behaviors with low optical loss (3 dB/mm).

Another important optical property related to molecular arrangement in a crystal is the polarization of emission. Nearly linearly polarized emission (polarization contrast as high as ~0.93) has been recently demonstrated from CNDPASDB crystal [32]. In this crystal, all of the CNDPASDB molecules are found to be parallel to each other with the identical conformation and orientation, as shown in Fig. 7.

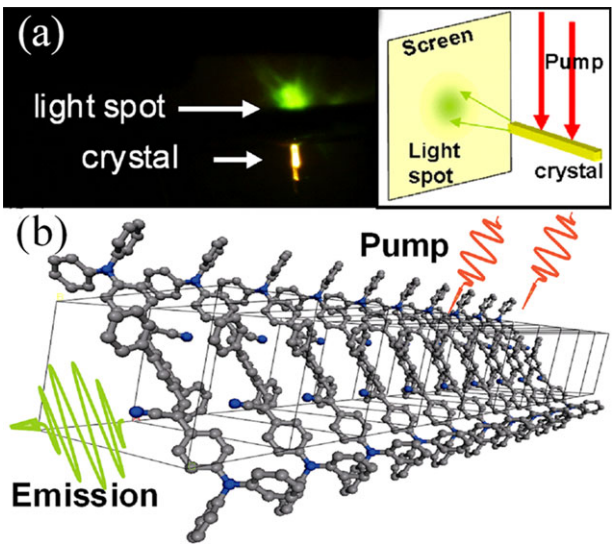


**Figure 7** (a) Photograph of a yellowish-green light spot from the CNDPASDB crystal. Inset, schematic representation of relative orientation for recording the PL spectra. (b) Molecular arrangement and configuration of the polarized emission from the crystals. (Reproduced with permission from [32]. Copyright 2010 Optical Society of America.)

It explains why highly polarized emission is produced. On the other hand, due to the intrinsic order present in the crystal, the transition dipole moments of the molecules exhibit optimal configuration with regard to the absorption and emission of light. This facilitates stimulated photon emission because the seed photons have been synchronized

in the polarization. Light polarization is enhanced and the lasing threshold is reduced when the photons are waveguided in the uniaxially oriented molecular crystals.

### 3.2. Two-photon excited upconversion stimulated emission from organic crystals

The properties of organic materials could be tailored to allow of novel approaches to make laser devices. Two-photon absorption (TPA), which have been applied in many research fields, is one such fantastic property. In TPA process, two photons of low energy (long wavelength) can be used to bridge the energy gap of the material instead of one high-energy (short wavelength) photon [193]. Then, near infrared (NIR) photon can be absorbed by a material that emits higher energy photon, providing an alternative approach to accomplish one kind of novel upconversion lasers, i.e., two-photon pumped (TPP) laser. Unlike that in second harmonic generation, phase-matching requirements are released [194, 195] in TPA process; and the lasing wavelength are tunable in the gain range of material. In two-photon pumping case, a pulsed laser, working in the NIR wavelength with hundreds femtoseconds duration, is usually used to create population inversion. As similar to single-photon pumping condition, the gain is determined by the population inversion, which is proportional to the volume density of excited states [196]. The distinct difference from the conventional laser is in light absorption. In single-photon pumping, the absorption is a linear optical process and described by the expression [197]:

$$\frac{dI}{dz} = -\alpha I \tag{1}$$

where, $I$ is the intensity of the incident light beam propagating along the z-axis, and z is a distance, $\alpha$ is the one-photon absorption coefficient. In a weak population rate regime. The gain is proportional to laser fluence ($g \sim \alpha I$).

In two-photon pumping, the absorption is proportional to the quadratic of laser energy, that is [198]:

$$\frac{dI}{dz} = -\beta I^2 \tag{2}$$

In the expression, $I$ is the intensity of the incident light beam propagating along the z-axis, $\beta$ is the two-photon absorption coefficient. The parameter $\beta$ can be further expressed as:

$$\beta = \frac{\delta N_A d_0 10^{-3}}{h\upsilon} \tag{3}$$

Here $\delta$ is the molecular TPA cross section in units of GM or $cm^4$ s $photon^{-1}$ $molecule^{-1}$ (1 GM = $10^{-50}$ $cm^4$ s $photon^{-1}$ $molecule^{-1}$), $N_A$ is Avogadro's number, and $d_0$ is the molar concentration of the absorbing molecules in units of M, $h\upsilon$ is the photon energy of the input light beam. For a number of efficient upconversion ASE crystals, their TPA cross section is generally range from 100 to 1000 GM.

Figure 8 shows the photograph of a DBASDMB crystal excited with a Ti:sapphire femtosecond laser at wavelength of 800 nm [143]. FWHM of photoluminescence spectrum collapse from 58 nm to 5 nm along with the increase of emission intensity. The threshold of TPP lasing is about only 15 times larger than that of single-photon pumping (1.68 $mJcm^{-2}pulse^{-1}$ for TPP lasing, 110 $\mu Jcm^{-2}pulse^{-1}$ for single photon pumping), which is much lower than that of expected. This allows lasing under much milder pumping condition, far below material degradation intensity. Sun et al. have further realized two-photon threshold for ASE

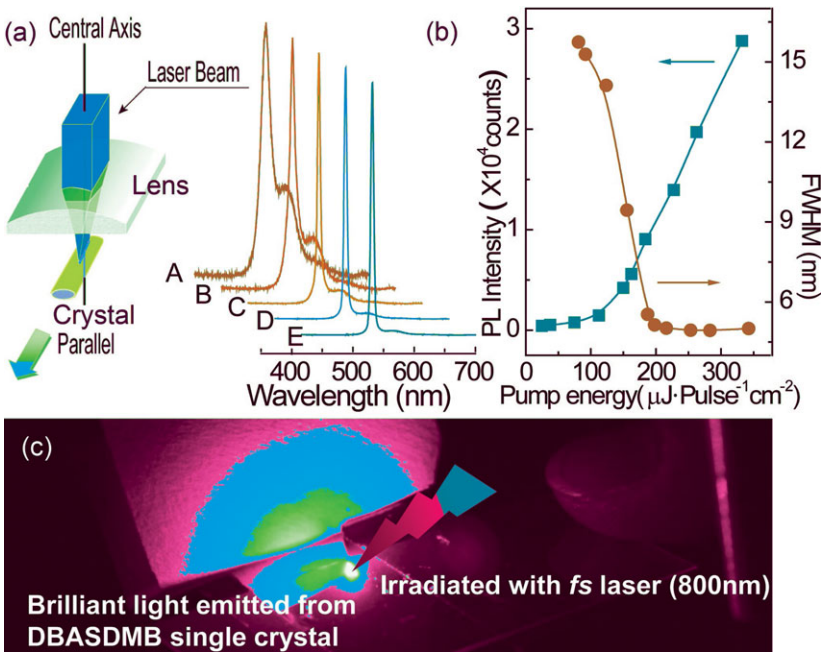


**Figure 8** (a) Setup for ASE measurement. (b) Upconverted normalized spontaneous emission and ASE spectra of DBASDMB. PL intensity and FWHM as function of the incident laser fluence. (c) Photograph of DBASDMB crystal under 800 nm femtosecond laser excitation. (Reproduced with permission [143]. Copyright 2010 Wiley-VCH Verlag GmbH & Co. KGaA, Weinheim.)

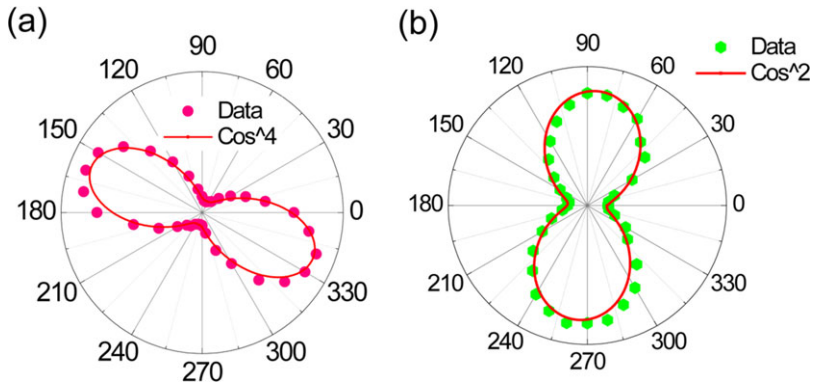


**Figure 9** The photoluminescence intensity of the crystal with respect to the polarization of the pump laser at excitation wavelength of (a) ex = 800 nm and (b) ex = 400 nm. (Reproduced with permission [30]. Copyright 2010 American Institute of Physics.)

as low as 0.29 mJ·pulse$^{-1}$·cm$^{-2}$ in Ph-TPA2 crystals [144]. The possible reason for unexpected results is that the two-photon absorption allows the pump light travel deeply into the sample, so more excited molecules inside of the crystals are excited; while the light penetration depth is very short for single photon excitation, only the molecules near the surface contribute to stimulated emission in single-photon condition. As a consequence, lasing under two photon pumping involves a much lower density of excited states, with advantages of low nonlinear loss mechanisms, such as singlet annihilation and charge separation [199].

As mentioned above, single crystals inherently possess long-range structural ordering and a remarkable linear optical anisotropy [200]. The ordered molecular packing results in an orientation-dependent linear optical properties in the materials, as well as nonlinear optical properties. Sun's group has performed detailed experimental studies on two-photon properties as a function of polarization of pump light, and revealed relationship between emission polarization and crystal structures in CNDPADSB crystals [30]. The results show that the polarization dependent properties in CNDPADSB crystals between the two-photon excitation (800 nm) and one-photon excitation (400 nm) are very different in distribution and direction, as shown in Fig. 9. The former generates a $\cos^4\theta$ distribution, while the latter gives rise to $\cos^2\theta$ distribution. And the most efficient pump polarization for 400 nm is nearly perpendicular to molecular long axis, while it's almost parallel for 800 nm. Similar polarization-dependent anisotropy in single crystals of cyanine-like dyes have been reported by Stryland et al. [201]. In contrast to the absorption, the emission polarization under the two-photon excitation is very similar to that of single-photon pumping [32]. They are both highly polarized in the same direction.

## 4. Lasing oscillation from single crystals

The optical gain properties have been well demonstrated with spectrally narrowed emission phenomena, such as ASE in the crystals. A real laser not only consists of a material capable of amplifying light, but also a resonator to introduce positive optical feedback [202, 203]. It repeatedly passes a resonant light field through the gain medium to establish a very intense, coherent optical field [14]. Two important properties of oscillating laser field are related with the parameters of resonator. One is the lasing frequency, which is imposed by the phase conservation after a roundtrip in the resonator. The second is transverse pattern of the laser beam, which is a consequence of the filtering role of the cavity. In every laser, a certain threshold condition must be reached to oscillate. In other words, oscillation only begins when the gain of the active material compensates the losses in the laser (e.g., losses due to output coupling). Once the critical inversion is reached, oscillation builds up from the spontaneous emission.

Laser resonators may have various shapes and architectures, such as microcavities, micro-rings, diffractive structures using optical gratings, distributed Bragg reflectors and photonic crystals. Depending on the type of materials, the choice of resonator and fabrication strategy may be very different. As for organic crystals, they have crystal facets and high refractive index, thus resonator fabrication differs from polymers. Applying optical resonators in organic single crystals have become one major research area in the last decade. How to obtain a proper single crystals and how to construct a high quality factor optical cavity for the single crystal are the challenges should be resolved before mass applications. There have been many efforts in developing simple and feasible technique to fabricate different type single-crystal-based resonators, and will be discussed in this section.

### *4.1. Lasing oscillation from crystals with naturally formed Fabry–Pérot (F-P) resonator*

The most natural resonator geometry for crystals is the plane parallel Fabry–Pérot resonator, which makes use of end crystal facets as reflective mirrors. For instance, lasing oscillation in monolithic single crystals of P6T demonstrated by Ichikawa et al. [94]. They prepared P6T with vertical crystal facets (i.e. the *XZ*-plane) on either crystal edge, forming a pair of F-P cavities. In this case, it demands that the crystal has optical quality facets and high refractive index, ensuring strong self-cavity optical confinement in the crystals. The laser emission spectrum is shown in Fig. 10. A progression of extremely narrow emission lines clearly appears around 689 nm with a threshold noted at

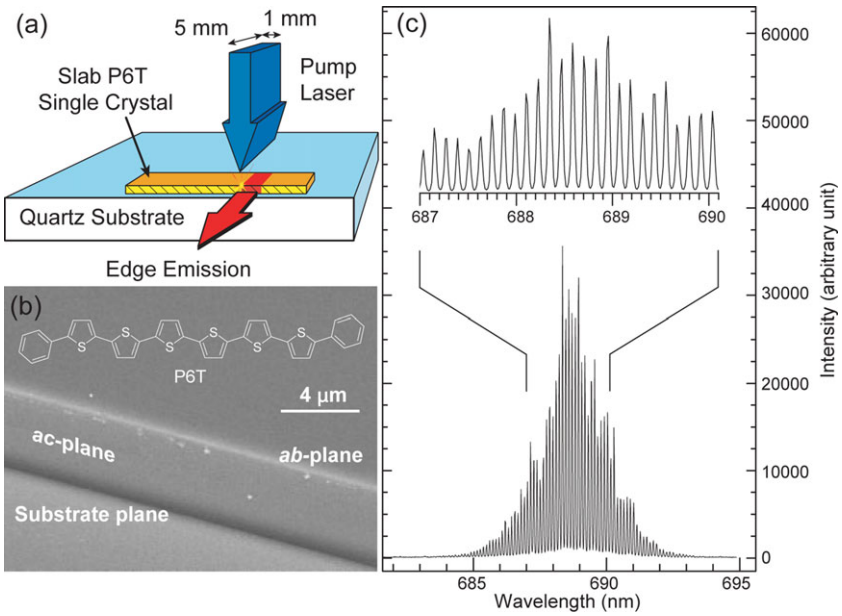


**Figure 10** Schematic of the laser structure with P6T crystal and lasing experiment setup. (b) SEM image of a P6T crystal. The crystal face corresponding to the XZ-plane. (c) Molecule structure of P6T and laser-induced light emission spectrum of a P6T crystal. (Reproduced with permission [94]. Copyright 2005 by WILEY-VCH Verlag GmbH & Co. KGaA, Weinheim.)

750 μJ $cm^{-2}$. The FWHM of the individual lines is narrowed to 38 pm, with an interval of 121 pm.

The optical resonator length is defined as the separation between the two ends (measured along the *Y*-axis). When the round trip optical path length is equal to an integer number of the light wavelength, constructive interference of light takes place inside the cavity. This is known as the resonant condition [204]:

$$nL = m\lambda \tag{4}$$

where n, L are the phase refractive index of crystal and round-trip distance, respectively, and m (an integer) is the order of mode. Laser oscillations have been observed from many other TPCOs crystals with clean cleaved facets [121, 205, 206]. These materials have high refractive index (more than 2.9 in crystals), according to the calculation of Yamao et al. [36]. The use of crystal facets is simple way to construct feedback resonator. However, the cavity length for this natural formed resonator is uncontrollable.

### *4.2. Whispering gallery mode lasing from crystalline microdisks*

Another kind optical cavity investigated constantly is whispering gallery mode (WGM) resonator, which provides a unique device geometry for realizing ultra-compact laser source and photonic circuit integration. Unlike F-P cavity, WGM structures utilize low-loss, total internal reflection of the optical mode along the circumference of the structure, which effectively reduces the volume of gain material required for lasing [207]. As a result, circularly resonant cavities provide much higher quality (Q) factors than lower reflection linear cavities. Organic crystal WGM resonators support strongly confined modes due to the large refractive index contrast between the resonator material and its surrounding. The resonator's diameter could be shrunk down to a few microns and integrated on a chip.

Two strategies are often adopted to make such structures: bottom-up synthesis and top-down fabrication. For example, inorganic crystal materials, such as ZnO nanostructures prepared by bottom-up synthesis, usually have a perfectly hexagonally shaped cross-section [208]. Light is reflected at the boundary between ZnO/air interface, and forms a closed loop in ZnO. This concept can be lent to organic crystal. However, it strongly depends on morphology of grown crystals. It is a challenge to get organic crystals with regular polygonal shapes. Instead, top-down fabricated crystalline microlaser is easy to control and for mass fabrication. Masumoto et al. fabricated microring structures by dry etching from thin film crystals of TPCO [209]. Laser oscillation of whispering gallery modes was observed in micro-ring structures at room temperature. They reported a 7 times reduction in threshold for the laser oscillation of a microring crystal compared with that of thin film materials. Sun and coworkers fabricated microdisk arrays of BP1T and BP2T single crystals using a combination method with improved lithography technique and reactive ion etching, as shown in (Fig. 11) [210]. Whispering gallery mode lasing oscillation is unambiguously observed from circle single crystal microdisks. Through analyzing the laser spectrum, they demonstrated that the investigated single crystals not only have very large refractive index (phase refractive index ~2.9) but also very large dispersion in refractive index. Because of high refractive index, it is possible to realized lasing when resonator is embedded in other medium, and convenient for integration in photonic integrated circuits (PICs). In addition, lasing oscillations in the regular polygonal cavity based on the BP2T crystals is also available. In polygonal microcavity, there exist many eigenmodes satisfying the condition of total internal bounce reflections at the cavity walls, similar as in circle disks. Thus, it is conventional for coupling with other photonic components, such as waveguide.

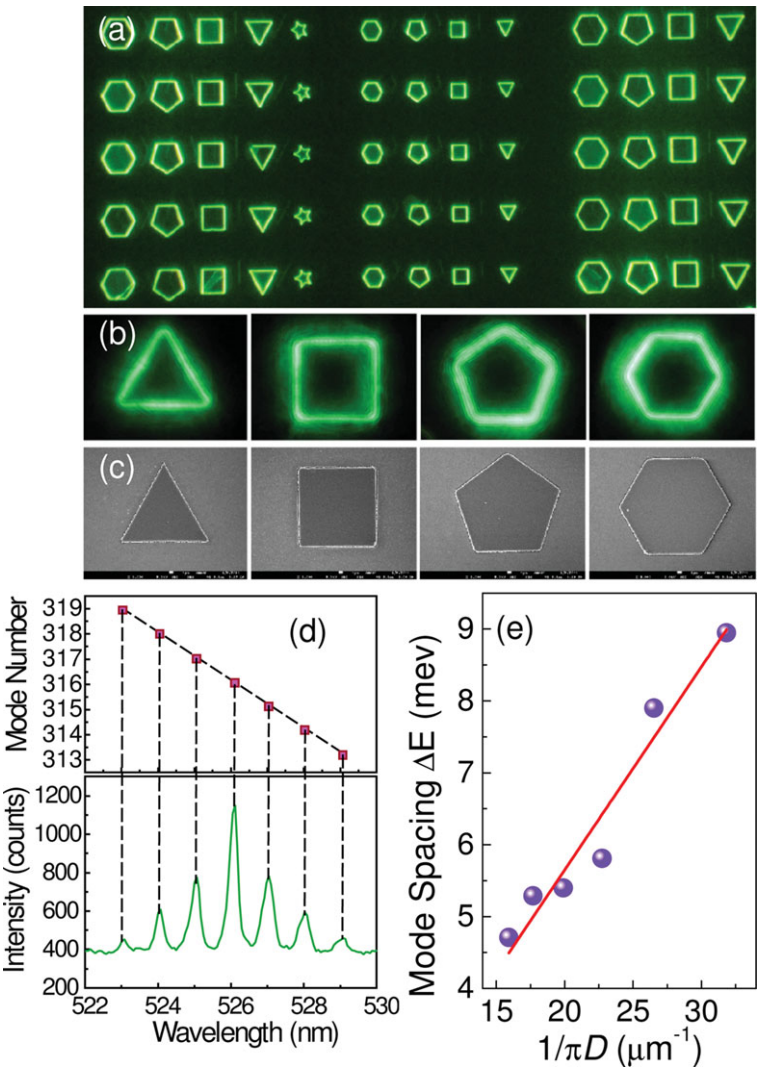


**Figure 11** (a)-(b) Fluorescence photograph of fabricated polygon BP2T microdisk arrays, including triangular, square, pentagonal, hexagonal and star. (c) Scanning electron microscope image of individual polygon BP2T microdisk. (d) Lasing spectrum at 34.1 nJ, and calculated WGM lasing mode numbers. (e) The mode spacing as a function of reciprocal of circle disk size. (Reproduced with permission [210]. Copyright 2012 by WILEY-VCH Verlag GmbH & Co. KGaA, Weinheim.)

### *4.3. Lasing from single crystals with waveguide distributed feedback*

Distributed feedback (DFB) is a very common feedback mechanism used for polymer lasers [211, 212]. In this scheme, feedback is provided by periodic change in refractive index. The scattered light from each corrugation can combine through constructive interference to create a "Bragg scattered" wave that also propagates within the film but in a different direction, when the period of the corrugations meet the requirement of Bragg scattering. The full description of such a mechanism has been described with the coupled mode theory by Kogelnik et al. [213]. The lasing wavelength λ is given by the Bragg expression [14],

$$2n_{eff}\Lambda = m\lambda \tag{5}$$

where Λ is the periodicity of the grating, m is the order Bragg reflection, and $n_{eff}$ is the effective refractive index of the waveguide, which is a geometrical average of the refractive indices of the layers of the waveguide and can be calculated through a solution of the Helmholtz wave equation for a planar multilayer structure.

A variety of fabrication schemes have been demonstrated to construct the DFB cavities, such as UV embossing, nanoimprint lithography for polymers [214]. For single crystals, different strategies have to be adapted to compatible with the features of crystals. Sun and coworkers have recently made use of laser interference ablation method to directly fabricate gratings in thin film organic crystals of BP2T (Fig. 12) [114]. The crystals act both as the gain medium and resonator. Strong distributed feedback lasing was demonstrated from these nanostructured crystal devices. Figure 12c shows the laser spectrum from the distributed feedback BP2T crystal laser. A progression of narrow emission lines clearly appear around 565 nm with a threshold at 25 $\mu Jcm^{-2}$.

In addition to the grating structure inside the crystals, they have fabricated lasers with an external feedback structure [215,216]. The gratings and the crystals are separately fabricated. It constitutes a DFB cavity through optical coupling between the BP2T crystal waveguide layer and the

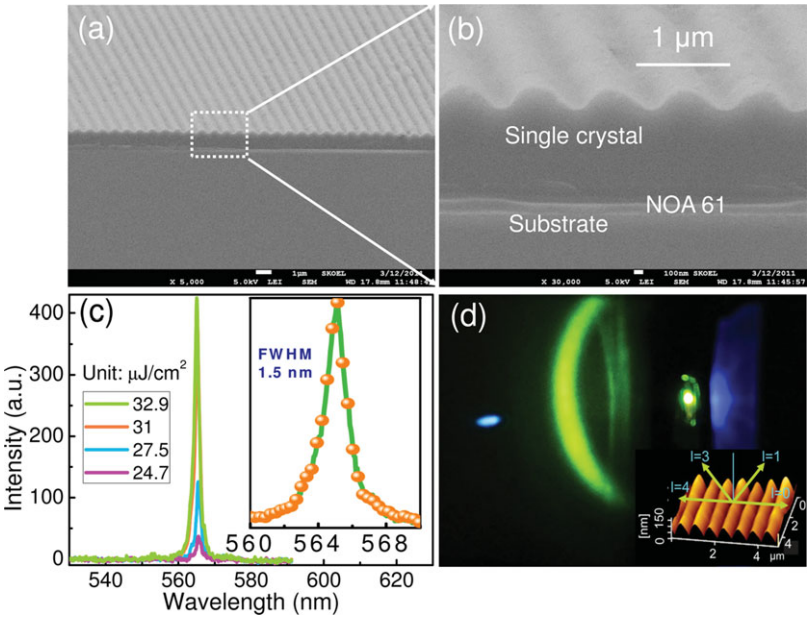


**Figure 12** (a) Image of thin film crystals fabricated with 800 nm period grating. b) Enlarged SEM image of side view. (c) Measured spectra of the lasing emission of the laser at different pump fluence, showing a center wavelength of about 565 nm. (d) Photographs of the operating single crystal laser based on 1D DFB structure. (Reproduced with permission [114]. Copyright 2012 by WILEY-VCH Verlag GmbH & Co. KGaA, Weinheim.)

S1805 photoresist grating structures on the top. The grating structure on top of the active polymer waveguide was produced by interference lithography, exposing photoresist to the interference pattern of two UV laser beams. The superiority for this structure is that avoids use of micromachining of crystals and takes advantage of their excellent waveguide properties, therefore greatly maintaining the intrinsic properties of crystal. This is crucial for improving device performance, especially for future electron injection. With this structure, "flexible" single-crystalline distributed feedback laser with ultrathin crystals with hundreds nanometers thickness is possible [215]. The fabricated "flexible" single-crystal laser could be bent with a radius of curvature less than 1 cm, and recover after more than 1000 times bending cycles without performance decline.

### 4.4. Planar microcavity lasers

As mentioned above, when a molecular species possesses a well-defined melting point and remains stable at the corresponding temperature, it is possible to grow crystals from the molten compounds. The advantage of this method is that it allows incorporating crystalline materials into desired structures [159, 217]. Anthracene is an example of material capable of melt-processing. Kena-Cohen and Forrest et al. have recently fabricated a crystalline anthracene into a 120-nm-thick microcavity, which is sandwiched between two 12-period differently SiNx/SiO2 distributed Bragg reflectors (Fig. 13). With this structure, they observed strong exciton-photon coupling (polariton) [218], which can undergo stimulated scattering that promises more energy-efficient generation of coherent light by 'polariton lasers'. Polariton laser operation has been demonstrated in optically and even electrically pumped semiconductor microcavities [219, 220], and such lasers can outperform their weak-coupling counterparts in that they have a lower threshold density [221–223]. For example, the polariton lasing threshold has been found to be as much as three orders of magnitude lower than that of conventional photon lasing in GaN microcavities [224]. Since Frenkel exciton have high binding energy, polaritons in organic semiconductors are highly stable at room temperature. Thus it is a great advantage to use organic semiconductor to explore polariton devices. Kéna-Cohen et al. have recently exploited room-temperature polartion laser with such kind of anthracene crystal cavity [225]. They clearly observed a threshold for nonlinear emission accompanied by a significant line narrowing, emission lifetime collapsing, as well as a redistribution of the polariton population. In principle, polariton laser does not require a population inversion and can exhibit 'zero-threshold' lasing characteristics. Therefore the required current density is much lower than that in conventional "photon laser", offering an optional direction to realize direct current injection lasers [219, 226, 227].

Another method to construct vertical cavities is deposition of dielectric mirrors directly on the both sides of crystals. Optical quality surfaces of crystals provide an opportunity to fabricate smooth dielectric mirrors. With reactive electron-beam deposition of dielectric mirrors on tetracene (TCN) crystals, Pisignano and coworkers demonstrated monolithic, light-emitting vertical TCN crystal microcavities [228]. However, cavity quality fabricated with this technique strongly relies on the morphology of crystal, making it limited to slab crystals and crystal thin films. On the other hand, the cavity length is hard to control, then difficult to adjust the cavity properties.

### 4.5. Lasing oscillation from low-dimensional organic crystal nanostructures

Miniaturization of laser devices is another important trend for applications in optical integration, where organic

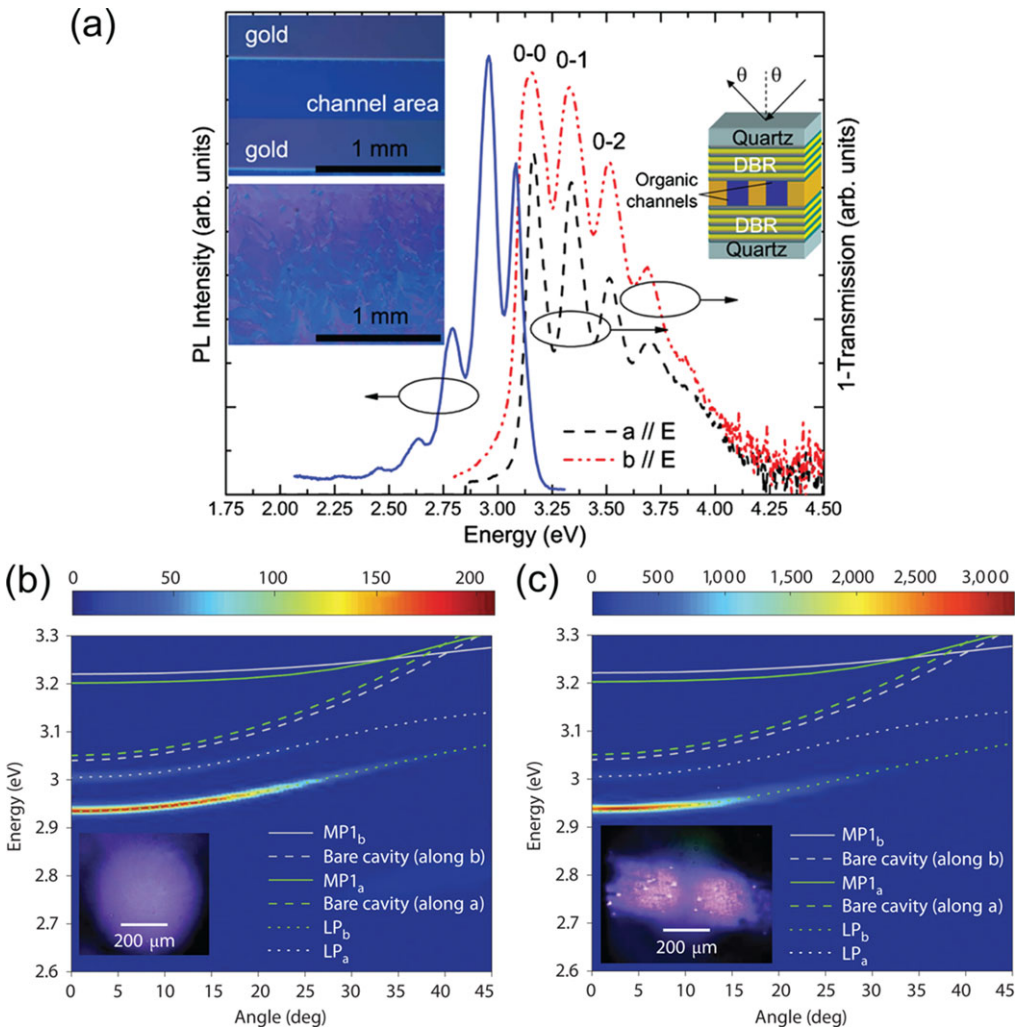


**Figure 13** (a)120 nm-thick anthracene single crystal, and corresponding inverse transmission (1-T) spectrum and photoluminescence spectrum. Reproduced with permission.[218] Copyright 2008 The American Physical Society. (b) Angle-resolved photoluminescence measured below threshold. (c) Angle-resolved photoluminescence measured above threshold. Emission is seen to still occur from the lower polariton branches and not the 'uncoupled' cavity, providing strong evidence for polariton lasing. (Reproduced with permission [225]. Copyright 2010, Nature Publishing Group.)

single-crystal nanostructures can find widely applying space [229–231]. Figure 14 exhibit some typical one dimensional crystalline nanomaterials. Compared with large size crystals, it is much easier to synthesize and with advantage of less defects. Physical vapor deposition has achieved great success in fabricating such kind of nanomaterials. For example, Yanagi et al. have prepared the crystalline para-sexiphenyl (p-6P) nanowires on KCl substrate [35], exhibiting excellent waveguide properties. Following their research, Quochi et al. observed lasing processes in individual self-assembled organic nanofibers grown on mica substrates (Fig. 15) [232], where lasing occurs in long nanofibers with randomly distributed scattering centers. It is also very easy to obtain nanowire with regular geometrical cross section. Single crystalline nanowires with quadrangular cross sections from 2,4,5-triphenylimidazole (TPI) [233], as well as 1,4-dimethoxy-2,5-di[[4]′-(methylthio)styryl]benzene (TDSB) [51] have been demonstrated, both showing Fabry–Pérot modes lasing. It is possible to prepare one dimensional nanostructures with different cross sections, which can affect the lasing behaviors. Yoon et al. investigated lasing behavior from the hollow rectangular nanotube optical microresonator of 5,10,15,20-tetra(4-pyridyl)-porphyrin ($H_2$TPyP) [234]. It exhibits a vibronic lasing action that combine two kinds of cavity mode: one is the Fabry–Pérot mode to resonate along the growth direction of the tube, and the other is the rectangular ring mode to resonate by wave guiding alongside sharp bending corners (Fig. 15). Moreover, organic structures are highly flexible, allowing micromanipulation for photonic device fabrication. As shown in Fig. 15, optical microring resonators is presented.

As mentioned in Sec. 4.4, strong coupling between photons and excitons in the solid state will result in the

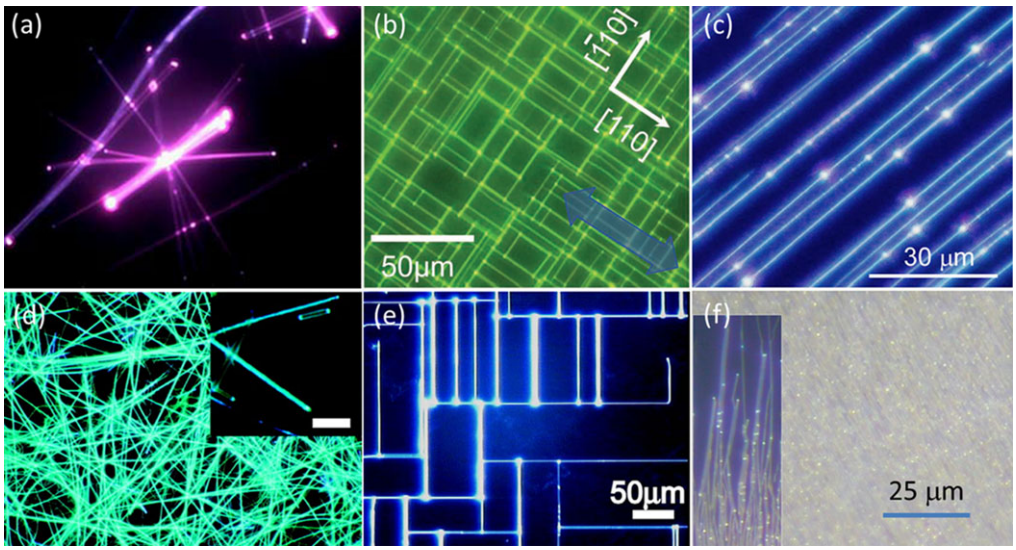


**Figure 14** (a) TPI nanowires deposited on a quartz wafer. (Reproduced with permission from [233]. Copyright 2008 WILEY-VCH Verlag GmbH & Co. KGaA, Weinheim.) (b) Image of epitaxially oriented BP2T needle-like crystals excited at $\lambda = 365$ nm. (Reproduced with permission from [123]. Copyright 2012 WILEY-VCH Verlag GmbH & Co. KGaA, Weinheim.) (c) Fluorescence micrograph of para-sexiphenyl nanofibers deposited on (001)-oriented muscovite mica. (Reproduced with permission from [113]. Copyright 2006 American Institute of Physics.) (d) PL image of the DPBT nanowires excited with the UV light source. (Reproduced with permission from [147]. Copyright 2011 American Chemical Society.) (e) Micro-PL image of BP1T needles on a KCl crystal. (Reproduced with permission from [229]. Copyright 2013 American Institute of Physics). (f) Para-hexaphenyl (p-6P)/$\alpha$-sexi-thiophene (6T) heterostructure nanofibers prepared y epitaxial growth. (Reproduced with permission from [230]. Copyright 2012 American Chemical Society.)

formation of exciton polaritons (EPs). EPs show remarkable propagation properties in comparison with uncoupled light, such as anomalously low group velocity, leading to substantially large refractive index. Nanowire with regular cross section can serve as high quality cavity, in which there may be strong coupling between photons and excitons. Takazawa et al. recently described the coupling of exciton polaritons (EPs) in 1D thiacyanine crystalline wire, and they demonstrated propagation of EPs over a few hundred micrometers at room temperature. Furthermore, they realized micrometer-scale photonic circuits based on the EPs [235, 236], providing a now platform to study the strong light–matter and photon–exciton interactions and towards novel EP devices.

## 5. Organic crystal light-emitting transistors: towards a current-injection laser

There is always a dream for researcher to realize an organic electrically driven laser. Historically, electroluminescence (EL) in organic materials have been observed as early as in 1950s [237]. In 1963, M. Pope et al. prepared a direct current cell using single crystals of anthracene, which was observed to fluoresce in the blue by applying 400 V across the specimen [238, 239]. In 1987, Tang and VanSlyke reported first organic light-emitting diode (OLED) [240]. In 1990, furthermore, Friend and co-workers proposed a polymer light-emitting diode (LED) [241]. To date, electroluminescence devices have achieved great success in commercial applications after intense research and development. However, lasing in organic semiconductor under direct electrical excitation has not been demonstrated yet. The main challenge that prevents the realization of electrical excitation laser is the additional losses occur in current driven structure [14]. The first source of losses associated with electrical pumping is the absorption by metallic electrodes, particularly when there has been overlap between the optical mode with the metallic electrodes. As a result, the threshold is greatly increased. It has been shown that the device lasing threshold was ~150 times greater than that of an otherwise similar metal-free device [242]. The second problem arise from the presence of polarons, which have broad absorption bands overlapping the emission that can absorb laser photons or quench singlet excitons. According to Rabe's examination, the polaron absorption cross section in a hole-transporting spiro bifluorene (S-TAD) compound is below $2.6 \times 10^{-18}$ cm$^{-2}$ between 560 and 660 nm [243]. The material absorption induced by polarons would be 11 cm$^{-1}$ at 500 nm. Organic light-emitting field-effect transistors (LEFET) are of high interest as many researchers consider the device architectures are capable of reducing exciton quenching and light absorption at the metallic electrodes to a minimum and realize high current density [244–248]. Due to different driving conditions with respect to standard OLED architectures [249] (see Fig. 16), the position of the recombination zone in an ambipolar organic LEFET can be moved within the transistor channel by the applied gate and drain voltages to be far away from the metal electrodes. As a consequence, it prevent exciton quenching and photon losses due to interaction with the metal electrodes [20, 245, 250–252]. These characteristics, in addition to the

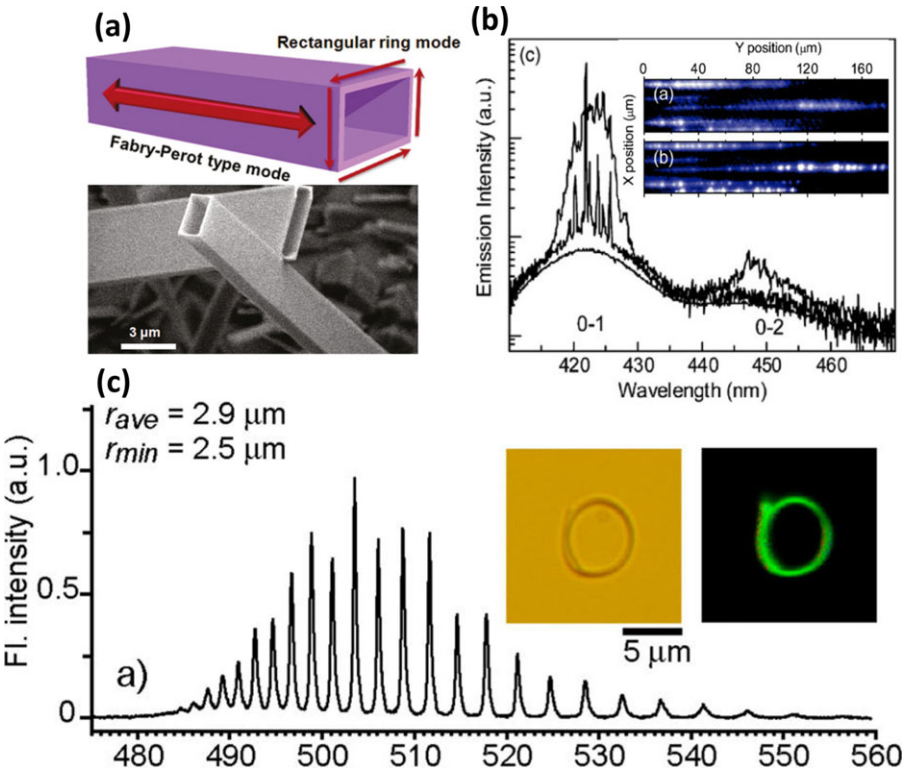


**Figure 15** (a) SEM images of H2TPyP rectangular microtubes and schematic diagram of the waveguide modes. (Reproduced with permission from [234]. Copyright © 2011 American Chemical Society). (b) Time integrated emission spectra of the nanofiber for different values of the excitation fluence. (Reproduced with permission from [113]. Copyright 2006 American Institute of Physics.) (c) Optical micrograph and FL microscopy image of a microring along with FL spectrum. (Reproduced with permission from [231]. Copyright 2013 American Chemical Society).

balanced electron and hole currents and to the higher charge mobility, have made LETs a widely researched device, particularly for applications that require high current densities. For detail in LEFETs, the reader is referred to previously published excellent reviews [244,245,253]. Here, we focus discussion on the single-crystal light-emitting field effect transistor.

In an optically pumped organic laser, the threshold of photon density to realize lasing is typically around 1 μJcm$^{-2}$. Assuming that the minimum pump intensity necessary for lasing in crystal is 1 μJcm$^{-2}$, 50% pump light is absorbed during the excitation and the photoluminescence quantum yield is 50%, then we can estimate the density of emitted photons (generated by photoluminescence) near the lasing threshold as $5 \times 10^{11}$ cm$^{-2}$. From these values, the minimum injection current density (that means without consideration of above-mentioned loss) required to reach the lasing threshold for electrically pumped laser can be estimated by the following equation [212]:

$$I_{th} \approx \frac{N_{th} \times q}{\chi \Phi_{in} \times \tau} \quad (6)$$

Here, $N_{th}$ is emitted photon density at lasing threshold ($5 \times 10^{11}$ cm$^{-2}$), q is electrical charge, $\Phi_{in}$ is internal quantum efficiency of electroluminescence, and $\tau$ is lifetime of excitons. If one assumes a singlet excitation ratio of $\chi = 0.25$ (Note 25% of singlet excitation is the theoretical limit, it is never achieved in reality [254]) and take typical value of organic crystal devcie for $\Phi_{in} = 5\%$ and $\tau = 5$ ns, respectively. Then the estimated lasing threshold in the injection current is around 1280 A/cm$^{-2}$, which is much higher than the typical limitation of OLEDs (1–10 Acm$^{-2}$). Note, it has not yet been taken into account any additional losses associated with contacts and carrier absorption, which need to be considered in electrically pumped structures.

With the advent of devices based on single crystals, the promotion of LETs' current density has experienced a significant leap. Takenobu et al. have recently demonstrated current density up to several kAcm$^{-2}$ (assuming 1 molecular layer (1 ML) as the accumulation layer thickness) in tetracene and rubrene single-crystal LETs without roll-off the luminescence efficiency [28]. The current density is 2 orders of magnitude larger than the maximum current density in conventional OLED devices. More recently, they further increased the current density of BP3T crystal LETs by inserting an electron-injection buffer layer in a current-confinement architecture [255]. The resultant maximum current density was 33 kA cm$^{-2}$, which is three orders of magnitude higher than that of OLEDs, and about one order higher than minimum required injection current. However, the achieved external quantum efficiency in the LETs is too low, and lasing emission have not been observed.

To achieve highly efficient LETs, not only high current density is needed, but also high external quantum efficiency. Unfortunately, a large number of the organic crystal LETs shows unipolar characteristics because of the unbalance in hole and electron mobility, making the number of injected electrons at the drain is much smaller than the number of holes injected at the source. As a result, the recombination occurs next to the metal electrode, leading to low emission efficiency. Thus, it needs

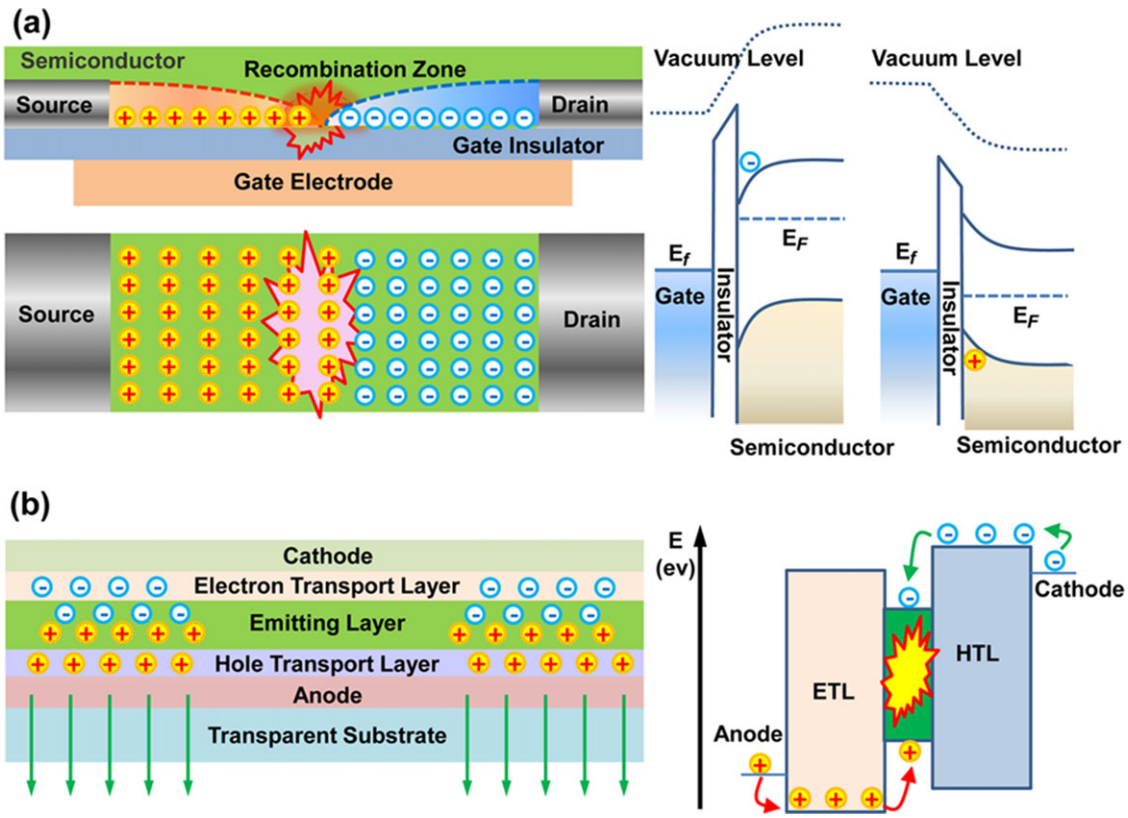


**Figure 16** Schematic representation of the device structures and of the main optoelectronic processes occurring in an light-emitting transistors (LET) and in an OLED. (a) Electrons and holes are injected from the drain and source contacts and recombine within the channel in a position controlled by the gate. Energy-level diagrams across the semiconductor/dielectric interface of organic transistors show the accumulation of negative carriers for positive gate-source voltages (n-channel transistor) and the accumulation of positive charge carriers for negative gate-source voltages (p-channel transistor). (b) Charges move vertically across the organic layers in OLEDs. The hole injection occurs in the hole transport layer (HTL) and the electron injection takes place in the electron transport layer (ETL). The radiative recombination occurs in the organic emitter.

to remedy the imbalance number of holes and electrons to obtain high exciton density. To achieve this goal, several factors have to be fulfilled. Firstly, the organic single-crystal must be able to transport both hole and electron, ideally with similar mobility and threshold voltage. Many organic crystals are ambipolar; that means they support both hole and electron transport [250, 256, 257]. However, the low electron affinity make them susceptible to show electron traps, which impede the electron transport, especially when exposed to oxygen and water [258]. It is a general route to increase the electron affinity by introducing electron-withdrawing group such as $-CF_3$ and $-CN$ [259]. Secondly, it is very important to minimize the electron traps by using an appropriate hydroxyl-free gate dielectric, such as divinyl-tetramethylsiloxane-bis(benzocyclobutene) derivative (BCB), polypropylene-co-1-butene and poly(methylmethacrylate) (PMMA) [260, 261]. Thirdly, it is crucial to select electrode with a suitable work function to match the crystal's highest occupied (HOMO) and lowest unoccupied (LUMO) molecular orbitals [262]. However, it is quite tedious when going to short channel length device. As an alternative way, air-stable electrode materials possess suitable energy level are highly desirable to improve injection of both hole and electrons. Finally, optimized device configurations are important to help increasing the achievable exciton density, for example, shortening the transistor channel to submicron lengths or adopting double gate transistor structure to control the holes and electrons transport.

A further and more serious issue with regard to current-driven laser is the loss associated with triplet state, which is inevitable under electrical excitation. The triplets generally have much longer lifetime in comparison to singlets. For example, time-resolved emission dynamics indicate that the lifetime of triplet exciton is 1.8 μs for pristine F8BT, and 4 μs for MEH-PPV [263], while the typical singlet lifetime is in nanosecond range. Stimulated emission occurs range from several to hundreds picoseconds [264, 265]. Due to triplets' relative long lifetime, they can act as meta-stable species, leading to triplet-singlet annihilation (TSA) and triplet state absorption (TA), and thus reducing the singlet density (for more details on triplets' property, please refer to Ref. [266–269]). So the triplets have to be "managed" or "suppressed", and the approaches include: 1) to choose

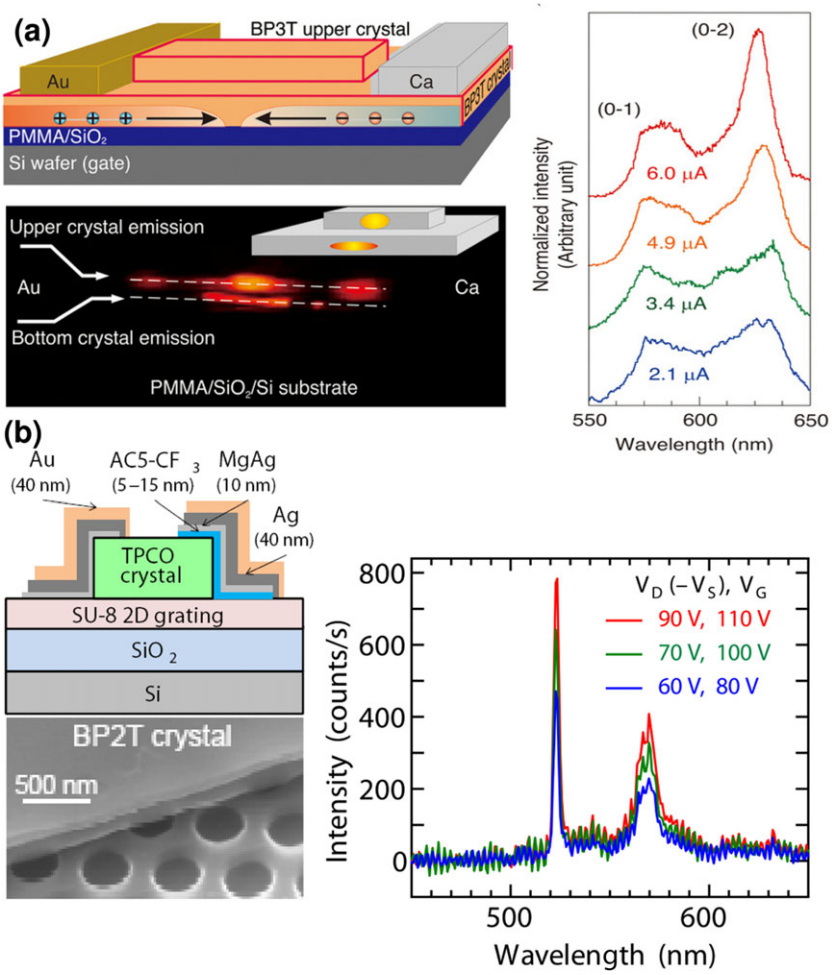


**Figure 17** (a) Organic light-emitting transistor with a single-crystal optical feedback resonator. Edge emission from the ambipolar SCLET of the bilaminar crystal recombination position was observed. Current dependence of electroluminescence spectra exhibited spectral narrowing at around 616 nm. (Reproduced with permission from [280]. Copyright 2010 Nature Publishing Group.) (b) Current-injected spectrally-narrowed emissions from an organic transistor using p-type organic crystals directly grown onto a two-dimensional polymer diffraction grating. (Reproduced with permission from [279]. Copyright 2012 WILEY-VCH Verlag GmbH & Co. KGaA, Weinheim.)

materials with gain and triplet absorption are spectrally separated [270, 271]; 2) to improve device operation to separate singlets from triplets in the time domain [272]; 3) to find an effective way to remove triplets or make use of them in lasing process, for example, by doping the crystal or developing co-crystal. Efficient energy transfer from a donor triplet state to an acceptor singlet state should not only increase the number of singlet excitons under electrical excitation but must also suppress triplet–triplet absorption [273–275]. By combining these techniques, the unwanted effects of triplet excitons in the recombination zone should be suppressed.

We have to mention that recently Yamao et al. improved the operating method of LETs by applying a square wave voltage to the gate electrode [276]. The alternating current voltage is very helpful to promote the charge injecion into the semiconductor layer. The device constitution is virtually unaltered, and stable metals such as gold and platinum can be used in the electrodes. In the varied square wave voltage operation, electrons and holes are injected alternately as well to cause the light emission by alternately switching the gate bias polarity. Both the charge recombination and emission take place more effectively by switching the gate bias more frequently and more suddenly.

Besides the varied device operation method, novel device configurations have to be explored to incorporate optical feedback resonator cavity in LETs to improve their performance. Gwinner et al. integrated a rib waveguide distributed feedback structure consisting of tantalum pentoxide ($Ta_2O_5$) within the channel [277]. The emitted light is coupled efficiently into the resonant mode of the DFB waveguide when the recombination zone of the LEFET is placed directly above the waveguide ridge. They observed the spectral narrowing from this device under the optical excitation. However, the hole mobility ($1.4 \times 10^{-3}$ $cm^2V^{-1}S^{-1}$) and electron mobility ($7 \times 10^{-4}$ $cm^2V^{-1}S^{-1}$) are both too low. The estimated current-injected singlet exciton density ($2–3 \times 10^8$ $cm^{-2}$) is at least about four orders of magnitude below the estimated requirements for lasing.

The manifestation of spectral narrowing under current-driven is particularly noteworthy because it might be a precursor phenomenon of lasing. With help of optical cavity, current-injected spectral narrowing emission (SNE) have been demonstrated recently. Yamao et al. achieved the SNE using a crystal of AC′7 (hole mobility: 0.12 $cm^2V^{-1}S^{-1}$) [278]. It is equipped with a diffraction grating on the silicon oxide gate insulator. When the device is operated by

applying square-wave alternating gate voltages, the spectral narrowing is observed at 556.3 nm with the FWHM of 2.05 nm. The estimated exciton density ($1.7 \times 10^{10}$ cm$^{-2}$) is 3 order lower than that ($2.9 \times 10^{13}$ cm$^{-2}$) under optical excitation. Similarly, with BP2T crystal on a two-dimensional polymer diffraction grating, they also demonstrated current-injected narrow emissions with 3.0 nm FWHM in LETs [279], as shown in Fig. 17. Also within an FET device, Bisri et al. introduced native Fabry–Pérot cavity [280]. It was reported that $\alpha$,$\omega$-bis(biphenylyl)terthiophene (BP3T) exhibits both high mobility (1.64 cm$^2$V$^{-1}$S$^{-1}$ for hole, 0.17 cm$^2$V$^{-1}$S$^{-1}$ for electron) and luminescence efficiency (80%) in single crystal LETs [124]. They choose single crystals of BP3T as the target material for waveguides, resonators, and couplers (as shown in Fig. 17). A narrow BP3T crystal with a pair of parallel crystal edges is laminated onto the surface of a larger BP3T to serve as a Fabry–Pérot resonator. The combination of single-crystal waveguides with optical feedback drastically reduces the lasing threshold under optical excitation and they observed a current density dependent spectral narrowing. The maximum current density they achieved was around 10 kA cm$^{-2}$. However, the origin of spectral narrowing is unclear, and need further evidence to clarify.

Single-crystal LETs are newly developed optoelectronic devices that combine with the switching mechanism of a transistor and an electroluminescent device. If the challenges (such as balance of hole and electron mobility, current density, luminance efficiency, and triplet losses, etc.) can be overcome, they may show promising applications in optical communication systems, advanced display technology, solid state lighting and electrically pumped organic lasers.

## 6. Conclusions and outlook

In this paper, we have reviewed the recent progress in the field of organic single crystals and their laser applications. Over the past decade, we have witnessed tremendous progress in crystal synthesis and device applications. Novel crystals simultaneously have both high photoluminescence efficiency and high carrier mobility have been exploited. Organic crystals have exhibited promising features for solid-state laser and amplifier application.

However, before the organic crystals can found their playground in real-world applications, many issues have to be addressed. Firstly, further exploration of organic single crystal with high optical response is necessary. At present, the optically lasing threshold is still quite high, making short operating lifetime. Typical maximum lifetime reported in literature is found to be $10^5$–$10^7$ pulses before the emission intensity decreases by a factor of two [216]. One possible solution to lower the ASE threshold is doping organic crystals [281, 282], allowing color tunability based on energy transfer and improved quantum efficiency and reduced ASE threshold by minimizing intermolecular interactions. Secondly, their mechanical performance and stability should be improved without influence on optoelectronic functions of materials in parallel with optical gain enhancement. For example, many of crystals are friable, making them difficult for cutting and polishing. On the other hand, specific encapsulation schemes can be used to prevent oxygen quenching or other detrimental effects to enhance the stability. It has been demonstrated that a careful encapsulation can enhance the lifetime by a factor of 2500 [283]. Thirdly, simple, and feasible techniques for mass devices construction are needed. The method usually used for polymers or inorganic single crystal could not be directly adopted because of their different physical properties. For this reason, compatible technology for large-area fabrication of single-crystal-based devices is desired.

As for the electrically pumped laser devices, both opportunities and challenges exist in crystals. In the organic crystal, the mobility can be several orders enhanced from their amorphous state, which is helpful to support high current densities. Meanwhile, high PL quantum yield can be maintained in the crystalline state trough proper control of molecular packing. The proposal of novel device structures, such as light emitting field effect transistor, have great suppressed electrode losses and polaron absorption, making them good candidates for electrically driven lasers. However, there are several issues in organic crystal LETs should be conquered: 1) unipolar transport properties because of unbalance in hole and electron mobility; 2) low external emission quantum efficiency; and 3) loss from triplet state. It is necessary to develop organic semiconductors with similar high mobility for ambipolar transport. At the same time, the material must have higher luminescence efficiency and optical gain. In addition to the use of novel materials, optimization or design of novel device structure is important to relieve the bottleneck. With a compatible feedback structure, optical properties in LET could be enhanced. As an alternative way, adoption of novel laser paradigm (such as incorporation of polariton cavity in the LET architecture), may open up a new exciting way to realize current inject lasers.

In summary, great efforts in the research of organic laser crystals have been made over past years. Due to their high gain and low optical losses, the organic crystals have become one important category of laser materials. In addition, they have cleaved crystal facets, highly polarized emission, high refractive indices, high index contrast to the cladding material and therefore they can have great potential applications in photonic integration. Since many novel functionalized semiconducting crystals and devices are currently being developed, we expect that organic crystals will play an important role in the future optoelectronic applications.

**Acknowledgements.** This work was supported by the Natural Science Foundation of China (NSFC) under Grants #61235004 and 51373064, and by "973" project under grant #2014CB921302 and 2011CB013003. H.H. Fang would like to acknowledge Prof. M. A. Loi, Dr. S.Z. Bisri and M. Abdu-Aguye for their help and discussion.

**Received:** 12 December 2013, **Revised:** 27 January 2014, **Accepted:** 6 February 2014

**Published online:** 3 March 2014

**Key words:** organic crystal, laser oscillation, optical resonator, light-emitting field effect transistor, stimulated emission.

**Hong-Hua Fang** obtained his B.Sc in 2006 in electronic science and technology in Jiin University. In 2009, he completed his Masters studies in the laboratory of Prof. Hong-Bo Sun at Jilin University. His thesis work focused on ultrafast dynamics and nonlinear optics of novel semiconductors. In 2013 he completed his Ph.D. research in the same group. His thesis work mainly focused on optoelectronics of organic semiconductor and their applications in laser devices. After that, he joined the Photophysics and OptoElectronics group of the Zernike Institute for Advanced Materials, University of Groningen (The Netherlands). His research focuses on photophysics and devices based on novel semiconductors materials.

**Jie Yang** received her Bachelors of Science degree in Microelectronics in 2006 from Jilin University, China. Then she joined Prof. Hong-bo Sun's research group. She completed her masters studies in 2008, and recived her Ph.D degree in 2011. In July 2011 she was appointed as an asistant professor in the college of Science, South China University of Technology. From Augest 2013, she worked in the Zernike Institute for Advanced Materials at the Univesity of Groningen, the Netherlands, as a research scientist.

**Jing Feng** received her B. S. and Ph. D. degrees in micro-electronics and solid-state electronics from Jilin University in 1997 and 2003, respectively. She worked as a postdoctoral researcher at RIKEN, Japan, from 2003 to 2006. She joined Jilin University in 2006, where she is a professor of College of Electronic Science and Engineering and State Key Laboratory on Integrated Optoelectronics. Her research focuses on the organic optoelectronic devices. She has published over 50 scientific papers in academic journals.

**Takeshi Yamao** received his Doctor of Engineering degree at Kyoto Institute of Technology (KIT) in 1999. He worked as a postdoctoral fellow at KIT (1999–2001) and Kyoto University (2001–2004). In 2004, he joined Prof. Hotta's research group as Research Associate in KIT, where he is currently Associate Professor. His current research interests include crystal growth of organic semiconductors, optical and electrical properties of the crystals, and applications of the crystals to devices.

**Shu Hotta** received his Doctor of Engineering degree at Kyoto University in 1988, while he was belonging to Matsushita Electric Industrial Co., Ltd. (currently, Panasonic Corporation). Since 2003, he has been a Professor of Laboratory of Polymer Physics, Department of Polymer Science and Engineering (currently, Department of Macromolecular Science and Engineering), Kyoto Institute of Technology (KIT). His research interests cover development of novel organic semiconductors and their optoelectronic device applications.

**Hong-Bo Sun** received his PhD from Jilin University in 1996. He worked as a postdoctoral researcher at the University of Tokushima, Japan, from 1996 to 2000, and then as an assistant professor in the Department of Applied Physics, Osaka University. He became a project leader in 2001. He was awarded by the Optical Science and Technology Society in 2002, and won an Outstanding Young Scientist Award issued by the minister of MEXT (Japan) in 2006. In 2005, he became a professor (Changjiang Scholar) at Jilin University. His research is focused on laser micronanofabrication, and its application in microoptics, micromachines, microfluids, and microsensors.

## References

[1] P. Heremans, Nature **444**, 828–831 (2006).
[2] E. Brock, P. Csavinszky, E. Hormats, H. Nedderman, D. Stirpe, and F. Unterleitner, J. Phys. Chem. **35**, 759–760 (1961).
[3] P. P. Sorokin and J. Lankard, IBM J. Res. Dev. **10**, 162–163 (1966).
[4] B. Soffer and B. McFarland, Appl. Phys. Lett. **10**, 266–267 (1967).
[5] N. Karl, Phys. Status Solidi A **13**, 651–655 (1972).
[6] O. Avanesjan, V. Benderskii, V. K. Brikenstein, V. Broude, L. Korshunov, A. Lavrushko, and I. Tartakovskii, Mol. Cryst. Liq. Cryst. **29**, 165–174 (1974).
[7] D. Moses, Appl. Phys. Lett. **60**, 3215–3216 (1992).
[8] N. Tessler, G. Denton, and R. Friend, Nature **382**, 695–697 (1996).
[9] F. Hide, M. A. Diaz-Garcia, and B. J. Schwartz, Science **273**, 1833–1836 (1996).
[10] F. Hide, M. A. Díaz-García, B. J. Schwartz, and A. J. Heeger, Acc. Chem. Res. **30**, 393–401 (1997).
[11] F. Hide, B. J. Schwartz, M. A. Díaz-García, and A. J. Heeger, Chem. Phys. Lett. **256**, 424–430 (1996).
[12] M. A. Díaz-García, F. Hide, B. J. Schwartz, M. R. Andersson, Q. Pei, and A. J. Heeger, Synth. Met. **84**, 455–462 (1997).

[13] N. D. Kumar, J. D. Bhawalkar, P. N. Prasad, F. E. Karasz, and B. Hu, Appl. Phys. Lett. **71**, 999–1001 (1997).
[14] I. D. W. Samuel and G. A. Turnbull, Chem. Rev. **107**, 1272–1295 (2007).
[15] S. Chenais and S. Forget, Polym. Int. **61**, 390–406 (2012).
[16] J. Herrnsdorf, Y. Wang, J. J. McKendry, Z. Gong, D. Massoubre, B. Guilhabert, G. Tsiminis, G. A. Turnbull, I. D. Samuel, and N. Laurand, Laser Photon. Rev. **7**, 1065–1078 (2013).
[17] I. D. Samuel, Nature **429**, 709–711 (2004).
[18] G. Kranzelbinder and G. Leising, Rep. Prog. Phys. **63**, and729–762 (2000).
[19] N. Tessler, Adv. Mater. **11**, 363–370 (1999).
[20] J. Clark and G. Lanzani, Nat. Photonics **4**, 438–446 (2010).
[21] M. D. McGehee and A. J. Heeger, Adv. Mater. **12**, 1655–1668 (2000).
[22] S. Forget and S. Chénais, Organic Materials for Solid-State Lasers, (Springer, 2013).
[23] C. Y. Liu and A. J. Bard, Acc. Chem. Res. **32**, 235–245 (1999).
[24] V. Podzorov, Mrs Bull. **38**, 15–24 (2013).
[25] R. W. I. de Boer, M. E. Gershenson, A. F. Morpurgo, and V. Podzorov, Phys. Status Solidi A **201**, 1302–1331 (2004).
[26] R. De Boer, T. Klapwijk, and A. Morpurgo, Appl. Phys. Lett. **83**, 4345–4347 (2003).
[27] V. Podzorov, E. Menard, A. Borissov, V. Kiryukhin, J. Rogers, and M. Gershenson, Phys. Rev. Lett. **93**, 86602, (2004).
[28] T. Takenobu, S. Z. Bisri, T. Takahashi, M. Yahiro, C. Adachi, and Y. Iwasa, Phys. Rev. Lett. **100**, 066601 (2008).
[29] K. Sawabe, T. Takenobu, S. Z. Bisri, T. Yamao, S. Hotta, and Y. Iwasa, Appl. Phys. Lett. **97**, 043307 (2010).
[30] H. H. Fang, J. Yang, R. Ding, Q. D. Chen, L. Wang, H. Xia, J. Feng, Y. G. Ma, and H. B. Sun, Appl. Phys. Lett. **97**, 101101 (2010).
[31] S. Tavazzi, L. Silvestri, L. Miozzo, A. Papagni, P. Spearman, S. Ianelli, A. Girlando, A. Camposeo, M. Polo, and D. Pisignano, Chemphyschem **11**, 429–434 (2010).
[32] H. H. Fang, Q. D. Chen, J. Yang, H. Xia, Y. G. Ma, H. Y. Wang, and H. B. Sun, Opt. Lett. **35**, 441–443 (2010).
[33] T. Yamao, Y. Taniguchi, K. Yamamoto, T. Miki, T. Ohira, and S. Hotta, Jpn. J. Appl. Phys. **47**, 4719–4723 (2008).
[34] S. Qu, Y. Li, L. Wang, Q. Lu, and X. Liu, Chem. Commun. **47**, 4207–4209 (2011).
[35] H. Yanagi and T. Morikawa, Appl. Phys. Lett. **75**, 187–189 (1999).
[36] T. Yamao, Y. Okuda, Y. Makino, and S. Hotta, J. Appl. Phys. **110**, 053113 (2011).
[37] T. Yamao, Y. Taniguchi, K. Yamamoto, T. Miki, S. Ota, S. Hotta, M. Goto, and R. Azumi, Jpn. J. Appl. Phys., Part 1 **46**, 7478–7482 (2007).
[38] K. Bando, S. Kumeta, F. Sasaki, and S. Hotta, Jpn. J. Appl. Phys. **50**, 101603 (2011).
[39] D. Rezzonico, S.-J. Kwon, H. Figi, O.-P. Kwon, M. Jazbinsek, and P. Günter, J. Phys. Chem. **128**, 124713 (2008).
[40] F. C. Spano and S. Mukamel, J. Phys. Chem. **95**, 7526–7540 (1991).
[41] M. Schwoerer and H. C. Wolf, Organic molecular solids, (Wiley. com, 2007), Chap. 6, p. 140.
[42] J. Gierschner, Y.-S. Huang, B. Van Averbeke, J. Cornil, R. H. Friend, and D. Beljonne, J. Phys. Chem. **130**, 044105 (2009).
[43] C. J. Bardeen, Mrs Bull. **38**, 65–71 (2013).
[44] M. Kasha, H. Rawls, and M. A. El-Bayoumi, Pure Appl. Chem. **11**, 371–392 (1965).
[45] F. C. Spano and C. Silva, Annu. Rev. Phys. Chem. **65**, and477–500 (2014).
[46] F. C. Spano, J. Phys. Chem. **118**, 981–994 (2003).
[47] S. Siddiqui and F. Spano, Chem. Phys. Lett. **308**, and99–105 (1999).
[48] F. C. Spano, Acc. Chem. Res. **43**, 429–439 (2009).
[49] F. C. Spano, Ann. Rev. Phys. Chem. **57**, 217–243 (2006).
[50] V. Shinto, P. S. Kyu, C. Santiago, C. F. Roland, R. Roland, M.-M. Begoña, W. Reinhold, P. S. Young, and G. Johannes, J. Phys. Chem. Lett. **4**, 1597–1602 (2013).
[51] Z. Z. Xu, Q. Liao, Q. Shi, H. L. Zhang, J. N. Yao, and H. B. Fu, Adv. Mater. **24**, OP216–OP220 (2012).
[52] J. Gierschner, L. Lüer, B. Milián-Medina, D. Oelkrug, and H.-J. Egelhaaf, J. Phys. Chem. Lett. **4**, 2686–2697 (2013).
[53] R. H. Dicke, Phys. Rev. **93**, 99–110 (1954).
[54] M. Scheibner, T. Schmidt, L. Worschech, A. Forchel, G. Bacher, T. Passow, and D. Hommel, Nature Phys. **3**, 106–110 (2007).
[55] N. Piovella, V. Beretta, G. R. M. Robb, and R. Bonifacio, Phys. Rev. A **68**, 021801 (2003).
[56] F. C. Spano and S. Mukamel, J. Phys. Chem. **91**, 683–700 (1989).
[57] F. Meinardi, M. Cerminara, A. Sassella, R. Bonifacio, and R. Tubino, Phys. Rev. Lett. **91**, 247401 (2003).
[58] H. Z. Wang, X. G. Zheng, F. L. Zhao, Z. L. Gao, and Z. X. Yu, Phys. Rev. Lett. **74**, 4079–4082 (1995).
[59] G. T. Noe II, J.-H. Kim, J. Lee, Y. Wang, A. K. Wójcik, S. A. McGill, D. H. Reitze, A. A. Belyanin, and J. Kono, Nature Phys. **8**, 219–224 (2012).
[60] V. Samartsev, S. Andrianov, Y. E. Sheibut, P. Zinoviev, and N. Silaeva, Laser Phys. **5**, 313–370 (1995).
[61] J. Knoester, J. Lumin. **53**, 101–104 (1992).
[62] A. Camposeo, M. Polo, S. Tavazzi, L. Silvestri, P. Spearman, R. Cingolani, and D. Pisignano, Phys. Rev. B **81**, 033306 (2010).
[63] J. Feldmann, G. Peter, E. O. Göbel, P. Dawson, K. Moore, C. Foxon, and R. J. Elliott, Phys. Rev. Lett. **59**, 2337–2340 (1987).
[64] S.-H. Lim, T. G. Bjorklund, F. C. Spano, and C. J. Bardeen, Phys. Rev. Lett. **92**, 107402 (2004).
[65] L. Cerdán, A. Costela, and I. García-Moreno, J. Opt. Soc. Am. B **27**, 1874–1877 (2010).
[66] D. Fichou, S. Delysse, and J. M. Nunzi, Adv. Mater. **9**, 1178–1181 (1997).
[67] M. Nagawa, R. Hibino, S. Hotta, H. Yanagi, M. Ichikawa, T. Koyama, and Y. Taniguchi, Appl. Phys. Lett. **80**, 544–546 (2002).
[68] M. Ichikawa, R. Hibino, M. Inoue, T. Haritani, S. Hotta, T. Koyama, and Y. Taniguchi, Adv. Mater. **15**, 213–217 (2003).
[69] K. Bando, T. Nakamura, Y. Masumoto, F. Sasaki, S. Kobayashi, and S. Hotta, J. Appl. Phys. **99**, 013518 (2006).

[70] P. A. Losio, C. Hunziker, and P. Gunter, Appl. Phys. Lett. **90**, 241103 (2007).
[71] W. J. Xie, Y. P. Li, F. Li, F. Z. Shen, and Y. G. Ma, Appl. Phys. Lett. **90**, 141110 (2007).
[72] M. Polo, A. Camposeo, S. Tavazzi, L. Raimondo, P. Spearman, A. Papagni, R. Cingolani, and D. Pisignano, Appl. Phys. Lett. **92**, 083311 (2008).
[73] H. H. Fang, Q. D. Chen, J. Yang, L. Wang, Y. Jiang, H. Xia, J. Feng, Y. G. Ma, H. Y. Wang, and H. B. Sun, Appl. Phys. Lett. **96**, 103508 (2010).
[74] H. H. Fang, Q. D. Chen, J. Yang, H. Xia, B. R. Gao, J. Feng, Y. G. Ma, and H. B. Sun, J. Phys. Chem. C **114**, 11958–11961 (2010).
[75] H. Wang, F. Li, I. Ravia, B. R. Gao, Y. P. Li, V. Medvedev, H. B. Sun, N. Tessler, and Y. G. Ma, Adv. Funct. Mater. **21**, 3770–3777 (2011).
[76] J. Yang, R. Ding, R. Wang, C. J. Liu, A. W. Li, Y. S. Yu, J. P. Wang, and H. Yang, Chem. Res. Chin. Univ. **27**, 862–865 (2011).
[77] D. Fichou, B. Bachet, F. Demanze, I. Billy, G. Horowitz, and F. Garnier, Adv. Mater. **8**, 500–504 (1996).
[78] G. Hernandez-Sosa, C. Simbrunner, and H. Sitter, Appl. Phys. Lett. **95**, 203301 (2009).
[79] D. Fichou, V. Dumarcher, and J. M. Nunzi, "One- and two-photon stimulated emission in oligothiophenes single crystals", presented at International Conference on Science and Technology of Synthetic Metals (ICSM 98) (Montpellier, France, Jul 12–18, 1998).
[80] G. Horowitz, P. Valat, F. Garnier, F. Kouki, and V. Wintgens, Opt. Mater. **9**, 46–52 (1998).
[81] H. Yanagi and A. Yoshiki, Appl. Phys. Lett. **84**, 4783–4785 (2004).
[82] F. Cordella, F. Quochi, M. Saba, A. Andreev, H. Sitter, N. S. Sariciftci, A. Mura, and G. Bongiovanni, Adv. Mater. **19**, 2252–2256 (2007).
[83] F. Quochi, A. Andreev, F. Cordella, R. Orru, A. Mura, G. Bongiovanni, H. Hoppe, H. Sitter, and N. S. Sariciftci, "Low-threshold blue lasing in epitaxially grown para-sexiphenyl nanofibers", presented at 6th International Conference on Excitonic Processes in Condensed Matter (EXCON 04), (Cracow, POLAND, Jul 06–09, 2004).
[84] S. Hotta, H. Kimura, S. A. Lee, and T. Tamaki, J. Heterocycl. Chem. **37**, 281–286 (2000).
[85] K. Shimizu, D. Hoshino, and S. Hotta, Appl. Phys. Lett. **83**, 4494–4496 (2003).
[86] H. Yanagi, A. Yoshiki, S. Hotta, and S. Kobayashi, Appl. Phys. Lett. **83**, 1941–1943 (2003).
[87] S. Kobayashi, F. Sasaki, H. Yanagi, S. Hotta, M. Ichikawa, and Y. Taniguchi, J. Lumin. **112**, 325–328 (2005).
[88] T. Katagiri, S. Ota, T. Ohira, T. Yamao, and S. Hotta, J. Heterocycl. Chem. **44**, 853–862 (2007).
[89] K. Bando, T. Nakamura, S. Fujiwara, Y. Masumoto, F. Sasaki, S. Kobayashi, Y. Shimoi, and S. Hotta, Phys. Rev. B **77**, 045205 (2008).
[90] S. Tavazzi, L. Miozzo, L. Silvestri, S. Mora, P. Spearman, M. Moret, S. Rizzato, D. Braga, A. K. D. Diaw, D. Gninguе-Sall, J. J. Aaron, and A. Yassar, Cryst. Growth Des. **10**, 2342–2349 (2010).
[91] S. Hotta and T. Yamao, J. Mater. Chem. **21**, 1295–1304 (2011).
[92] H. Mizuno, U. Haku, Y. Marutani, A. Ishizumi, H. Yanagi, F. Sasaki, and S. Hotta, Adv. Mater. **24**, 5744–5749 (2012).
[93] H. Yanagi, A. Yoshiki, S. Hotta, and S. Kobayashi, J. Appl. Phys. **96**, 4240–4244 (2004).
[94] M. Ichikawa, R. Hibino, M. Inoue, T. Haritani, S. Hotta, K. Araki, T. Koyama, and Y. Taniguchi, Adv. Mater. **17**, 2073–2077 (2005).
[95] K. Shimizu, Y. Mori, and S. Hotta, J. Appl. Phys. **99**, 063505 (2006).
[96] T. Yamao, S. Ota, T. Miki, S. Hotta, and R. Azumi, "Improved sublimation growth of single crystals of thiophene/phenylene co-oligomers", presented at 7th International Conference on Nano-Molecular Electronics (ICNME2006), Kobe, JAPAN, Dec 12–15, Mar 3, 2006.
[97] T. Yamao, K. Yamamoto, Y. Taniguchi, and S. Hotta, Appl. Phys. Lett. **91**, 201117 (2007).
[98] X. H. Zhu, D. Gindre, N. Mercier, P. Frere, and J. M. Nunzi, Adv. Mater. **15**, 906–909 (2003).
[99] Z. Q. Xie, B. Yang, F. Li, G. Cheng, L. L. Liu, G. D. Yang, H. Xu, L. Ye, M. Hanif, S. Y. Liu, D. G. Ma, and Y. G. Ma, J. Am. Chem. Soc. **127**, 14152–14153 (2005).
[100] W. J. Xie, F. Li, H. Wang, Z. Q. Xie, F. Z. Shen, Y. G. Ma, W. Lu, D. K. Zhang, and D. G. Ma, Appl. Optics **46**, 4431–4433 (2007).
[101] R. Kabe, H. Nakanotani, T. Sakanoue, M. Yahiro, and C. Adachi, Adv. Mater. **21**, 4034–4038 (2009).
[102] D. Fichou, F. Demanze, G. Horowitz, R. Hajlaoui, M. Constant, and F. Gamier, Synth. Met. **85**, 1309–1312 (1997).
[103] G. Horowitz, F. Kouki, A. E. Kassmi, P. Valat, V. Wintgens, and F. Garnier, Adv. Mater. **11**, 234–238 (1999).
[104] D. Fichou, M. P. te Ulade-Fichou, G. Horowitz, and F. Demanze, Adv. Mater. **9**, 75–80 (1997).
[105] G. Horowitz, S. Romdhane, H. Bouchriha, P. Delannoy, J.-L. Monge, F. Kouki, and P. Valat, Synth. Met. **90**, 187–192 (1997).
[106] D. Fichou, J. Mater. Chem. **10**, 571–588 (2000).
[107] H. Yanagi and S. Okamoto, Appl. Phys. Lett. **71**, 2563–2565 (1997).
[108] A. Andreev, G. Matt, C. J. Brabec, H. Sitter, D. Badt, H. Seyringer, and N. S. Sariciftci, Adv. Mater. **12**, 629–633 (2000).
[109] A. Andreev, F. Quochi, A. Kadashchuk, H. Sitter, C. Winder, H. Hoppe, S. Sariciftci, A. Mura, and G. Bongiovanni, Phys. Status Solidi A **201**, 2288–2293 (2004).
[110] F. Quochi, A. Andreev, F. Cordella, R. Orru, A. Mura, G. Bongiovanni, H. Hoppe, H. Sitter, and N. S. Sariciftci, J. Lumin. **112**, 321–324 (2005).
[111] A. Kadashchuk, A. Andreev, H. Sitter, N. S. Sariciftci, Y. Skryshevski, Y. Piryatinski, I. Blonsky, and D. Meissner, Adv. Funct. Mater. **14**, 970–978 (2004).
[112] H. Yanagi, T. Ohara, and T. Morikawa, Adv. Mater. **13**, 1452–1455 (2001).
[113] F. Quochi, F. Cordella, A. Mura, G. Bongiovanni, F. Balzer, and H. G. Rubahn, Appl. Phys. Lett. **88**, 041106 (2006).
[114] H. H. Fang, R. Ding, S. Y. Lu, J. Yang, X. L. Zhang, R. Yang, J. Feng, Q. D. Chen, J. F. Song, and H. B. Sun, Adv. Funct. Mater. **22**, 33–38 (2012).
[115] S. Hotta, S. Lee, and T. Tamaki, J. Heterocycl. Chem. **37**, 25–29 (2009).
[116] S. Hotta, J. Heterocycl. Chem. **38**, 923–927 (2009).

[117] S. Hotta and T. Katagiri, J. Heterocycl. Chem. **40**, 845–850 (2009).
[118] T. Katagiri, S. Ota, T. Ohira, T. Yamao, and S. Hotta, J. Heterocycl. Chem. **44**, 853–862 (2007).
[119] T. Dingemans, A. Bacher, M. Thelakkat, L. Pedersen, E. Samulski, and H.-W. Schmidt, Synth. Met. **105**, 171–177 (1999).
[120] R. Hibino, M. Nagawa, S. Hotta, M. Ichikawa, T. Koyama, and Y. Taniguchi, Adv. Mater. **14**, 119–122 (2002).
[121] M. Ichikawa, K. Nakamura, M. Inoue, H. Mishima, T. Haritani, R. Hibino, T. Koyama, and Y. Taniguchi, Appl. Phys. Lett. **87**, 221113 (2005).
[122] Y. Yomogida, T. Takenobu, H. Shimotani, K. Sawabe, S. Z. Bisri, T. Yamao, S. Hotta, and Y. Iwasa, Appl. Phys. Lett. **97**, 173301 (2010).
[123] H. Mizuno, I. Ohnishi, H. Yanagi, F. Sasaki, and S. Hotta, Adv. Mater. **24**, 2404–2408 (2012).
[124] S. Z. Bisri, T. Takenobu, Y. Yomogida, H. Shimotani, T. Yamao, S. Hotta, and Y. Iwasa, Adv. Funct. Mater. **19**, 1728–1735 (2009).
[125] C. C. Wu, O. J. Korovyanko, M. C. Delong, Z. V. Vardeny, and J. P. Ferraris, Synth. Met. **139**, 735–738 (2003).
[126] Y. P. Li, F. Li, H. Y. Zhang, Z. Q. Xie, W. J. Xie, H. Xu, B. Li, F. Z. Shen, L. Ye, M. Hanif, D. G. Ma, and Y. G. Ma, Chem. Commun. 231–233 (2007).
[127] Y. P. Li, F. Z. Shen, H. Wang, F. He, Z. Q. Xie, H. Y. Zhang, Z. M. Wang, L. L. Liu, F. Li, M. Hanif, L. Ye, and Y. G. Ma, Chem. Mater. **20**, 7312–7318 (2008).
[128] Z. Q. Xie, L. L. Liu, B. Yang, G. D. Yang, L. Ye, M. Li, and Y. G. Ma, Cryst. Growth Des. **5**, 1959–1964 (2005).
[129] Z. Q. Xie, H. Wang, F. Li, W. J. Xie, L. L. Liu, B. Yang, L. Ye, and Y. G. Ma, Cryst. Growth Des. **7**, 2512–2516 (2007).
[130] H. Wang, Z. Q. Xie, B. Yang, F. Z. Shen, Y. P. Li, and Y. G. Ma, CrystEngComm **10**, 1252–1257 (2008).
[131] Z. Q. Xie, W. J. Xie, F. Li, L. L. Liu, H. Wang, and Y. G. Ma, J. Phys. Chem. C **112**, 9066–9071 (2008).
[132] Z. Q. Xie, B. Yang, L. L. Liu, M. Li, D. Lin, Y. G. Ma, G. Cheng, and S. Y. Liu, J. Phys. Org. Chem. **18**, 962–973 (2005).
[133] S. Varghese, S.-J. Yoon, E. M. Calzado, S. Casado, P. G. Boj, M. A. Díaz-García, R. Resel, R. Fischer, B. Milián-Medina, R. Wannemacher, S. Y. Park, and J. Gierschner, Adv. Mater. **24**, 6473–6478 (2012).
[134] S. J. Yoon, S. Varghese, S. K. Park, R. Wannemacher, J. Gierschner, and S. Y. Park, Adv. Opt. Mater. **1**, 232–237 (2013).
[135] S. Park, O.-H. Kwon, S. Kim, S. Park, M.-G. Choi, M. Cha, S. Y. Park, and D.-J. Jang, J. Am. Chem. Soc. **127**, 10070–10074 (2005).
[136] J. E. Kwon and S. Y. Park, Adv. Mater. **23**, 3615–3642 (2011).
[137] B. H. Cumpston, S. P. Ananthavel, S. Barlow, D. L. Dyer, J. E. Ehrlich, L. L. Erskine, A. A. Heikal, S. M. Kuebler, I. Y. S. Lee, D. McCord-Maughon, J. Q. Qin, H. Rockel, M. Rumi, X. L. Wu, S. R. Marder, and J. W. Perry, Nature **398**, 51–54 (1999).
[138] Q. D. Zheng, S. K. Gupta, G. S. He, L. S. Tan, and P. A. N. Prasad, Adv. Funct. Mater. **18**, 2770–2779 (2008).
[139] J. Benedict and P. Coppens, J. Phys. Chem. A **113**, 3116–3120 (2009).
[140] S. Kawata, H. B. Sun, T. Tanaka, and K. Takada, Nature **412**, 697–698 (2001).
[141] W. Denk, J. Strickler, and W. Webb, Science **248**, 73–76 (1990).
[142] C. Bauer, B. Schnabel, E. B. Kley, U. Scherf, H. Giessen, and R. F. Mahrt, Adv. Mater. **14**, 673–676 (2002).
[143] H. Xia, J. Yang, H. H. Fang, Q. D. Chen, H. Y. Wang, X. Q. Yu, Y. G. Ma, M. H. Jiang, and H. B. Sun, Chemphyschem **11**, 1871–1875 (2010).
[144] Q. D. Chen, H. H. Fang, B. Xu, J. Yang, H. Xia, F. P. Chen, W. J. Tian, and H. B. Sun, Appl. Phys. Lett. **94**, 201113 (2009).
[145] H. H. Fang, B. Xu, Q. D. Chen, R. Ding, F. P. Chen, J. Yang, R. Wang, W. J. Tian, J. Feng, H. Y. Wang, and H. B. Sun, IEEE J. Quantum Electron. **46**, 1775–1781 (2010).
[146] F. Gao, Q. Liao, Z.-Z. Xu, Y.-H. Yue, Q. Wang, H.-L. Zhang, and H.-B. Fu, Angew. Chem. **49**, 732–735 (2010).
[147] C. Zhang, C. L. Zou, Y. L. Yan, R. Hao, F. W. Sun, Z. F. Han, Y. S. Zhao, and J. N. Yao, J. Am. Chem. Soc. **133**, 7276–7279 (2011).
[148] J. Hui and K. Christian, Mrs Bull. **38**, 28–33 (2013).
[149] S. J. Kwon, C. Hunziker, O. P. Kwon, M. Jazbinsek, and P. Gunter, Cryst. Growth Des. **9**, 2512–2516 (2009).
[150] H. Shang, H. Wang, N. Gao, F. Z. Shen, X. J. Li, and Y. G. Ma, CrystEngComm **14**, 869–874 (2012).
[151] R. J. Li, W. P. Hu, Y. Q. Liu, and D. B. Zhu, Acc. Chem. Res. **43**, 529–540 (2010).
[152] Y. H. Tong, Q. X. Tang, H. T. Lemke, K. Moth-Poulsen, F. Westerlund, P. Hammershoj, K. Bechgaard, W. P. Hu, and T. Bjornholm, Langmuir **26**, 1130–1136 (2010).
[153] N. Zaitseva, L. Carman, A. Glenn, J. Newby, M. Faust, S. Hamel, N. Cherepy, and S. Payne, J. Cryst. Growth. **314**, 163–170 (2011).
[154] O. Goto, S. Tomiya, Y. Murakami, A. Shinozaki, A. Toda, J. Kasahara, and D. Hobara, Adv. Mater. **24**, 1117–1122 (2012).
[155] C. Liu, T. Minari, Y. Li, A. Kumatani, M. V. Lee, S. H. A. Pan, K. Takimiya, and K. Tsukagoshi, J. Mater. Chem. **22**, 8462–8469 (2012).
[156] I. Markov, Crystal growth for beginners: fundamentals of nucleation, crystal growth and epitaxy (World Scientific Pub Co Inc, 2003).
[157] Y. Inada, T. Yamao, M. Inada, T. Itami, and S. Hotta, Synth. Met. **161**, 1869–1877 (2011).
[158] T. Yamao, T. Miki, H. Akagami, Y. Nishimoto, S. Ota, and S. Hotta, Chem. Mater. **19**, 3748–3753 (2007).
[159] H. Figi, M. Jazbinsek, C. Hunziker, M. Koechlin, and P. Gunter, Opt. Express **16**, 11310–11327 (2008).
[160] H. Figi, M. Jazbinsek, C. Hunziker, M. Koechlin, and P. Gunter, J. Opt. Soc. Am. B **26**, 1103–1110 (2009).
[161] O. P. Kwon, B. Ruiz, A. Choubey, L. Mutter, A. Schneider, M. Jazbinsek, V. Gramlich, and P. Gunter, Chem. Mater. **18**, 4049–4054 (2006).
[162] J. Czochralski, Z. Phys. Chemie **92**, 219–221 (1918).
[163] M. Arivanandhan, K. Sankaranarayanan, C. Sanjeeviraja, A. Arulchakkaravarthi, and P. Ramasamy, J. Cryst. Growth. **281**, 596–603 (2005).

[164] C. Kloc, P. Simpkins, T. Siegrist, and R. Laudise, J. Cryst. Growth. **182**, 416–427 (1997).
[165] R. Laudise, C. Kloc, P. Simpkins, and T. Siegrist, J. Cryst. Growth. **187**, 449–454 (1998).
[166] C. Kloc, T. Siegrist, and J. Pflaum, in Springer Handbook of Crystal Growth, (2010), pp. 845–867.
[167] Y. S. Zhao, C. A. Di, W. S. Yang, G. Yu, Y. Q. Liu, and J. N. Yao, Adv. Funct. Mater. **16**, 1985–1991 (2006).
[168] T. Yamao, S. Ota, T. Miki, S. Hotta, and R. Azumi, Thin Solid Films **516**, 2527–2531 (2008).
[169] T. Yamao, K. Juri, A. Kamoi, and S. Hotta, Org. Electron. **10**, 1241–1247 (2009).
[170] A. Choubey, O. P. Kwon, M. Jazbinsek, and P. Gunter, Cryst. Growth Des. **7**, 402–405 (2007).
[171] Y. W. Huang, R. J. Yuan, and S. M. Zhou, J. Mater. Chem. **22**, 883–888 (2012).
[172] B. Chapman, A. Checco, R. Pindak, T. Siegrist, and C. Kloc, J. Cryst. Growth. **290**, 479–484 (2006).
[173] J. Yang, H. H. Fang, R. Ding, S. Y. Lu, Y. L. Zhang, Q. D. Chen, and H. B. Sun, J. Phys. Chem. C **115**, 9171–9175 (2011).
[174] H. Wang, F. Li, B. Gao, Z. Xie, S. Liu, C. Wang, D. Hu, F. Shen, Y. Xu, H. Shang, Q. Chen, Y. Ma, and H. Sun, Cryst. Growth Des. **9**, 4945–4950 (2009).
[175] H.-H. Fang, S.-Y. Lu, L. Wang, R. Ding, H.-Y. Wang, J. Feng, Q.-D. Chen, and H.-B. Sun, Org. Electron. **14**, 389–395 (2013).
[176] K. Pernstich, S. Haas, D. Oberhoff, C. Goldmann, D. Gundlach, B. Batlogg, A. Rashid, and G. Schitter, J. Appl. Phys. **96**, 6431–6438 (2004).
[177] M. A. Spackman, Phys. Scr. **87**, 048103 (2013).
[178] M. Curtis, J. Cao, and J. Kampf, J. Am. Chem. Soc. **126**, 4318–4328 (2004).
[179] S. Hotta, M. Goto, and R. Azumi, Chem. Lett. **36**, 270–271 (2007).
[180] J. Cornil, D. Beljonne, J. P. Calbert, and J. L. Brédas, Adv. Mater. **13**, 1053–1067 (2001).
[181] G. Johannes and P. S. Young, J. Mater. Chem. C **1**, 5818–5832 (2013).
[182] Y. Dong, B. Xu, J. Zhang, X. Tan, L. Wang, J. Chen, H. Lv, S. Wen, B. Li, L. Ye, B. Zou, and W. Tian, Angew. Chem. **51**, 10782–10785 (2012).
[183] C. Wu, M. DeLong, Z. Vardeny, and J. Ferraris, Synth. Met. **137**, 939–941 (2003).
[184] J. Luo, Z. Xie, J. Lam, L. Cheng, B. Tang, H. Chen, C. Qiu, H. Kwok, X. Zhan, Y. Liu, and D. Zhu, Chem. Commun. 1740–1741 (2001).
[185] Y. Hong, J. Lam, and B. Tang, Chem. Soc. Rev. **40**, 5361–5388 (2011).
[186] Y. Hong, J. Lam, and B. Tang, Chem. Commun. 4332–4353 (2009).
[187] B.-K. An, J. Gierschner, and S. Park, Acc. Chem. Res. **45**, 544–554 (2012).
[188] J. Zhang, B. Xu, J. Chen, S. Ma, Y. Dong, L. Wang, B. Li, L. Ye, and W. Tian, Adv. Mater. **26**, 739–745 (2014).
[189] S. Hotta and M. Goto, Adv. Mater. **14**, 498–501 (2002).
[190] S. Hotta, M. Goto, R. Azumi, M. Inoue, M. Ichikawa, and Y. Taniguchi, Chem. Mater. **16**, 237–241 (2004).
[191] X. J. Zhang, J. S. Jie, W. F. Zhang, C. Y. Zhang, L. B. Luo, Z. B. He, X. H. Zhang, W. J. Zhang, C. S. Lee, and S. T. Lee, Adv. Mater. **20**, 2427–2432 (2008).
[192] Y. X. Xu, H. Y. Zhang, F. Li, F. Z. Shen, H. Wang, X. J. Li, Y. Yu, and Y. G. Ma, J. Mater. Chem. **22**, 1592–1597 (2012).
[193] M. Pawlicki, H. A. Collins, R. G. Denning, and H. L. Anderson, Angew. Chem. **48**, 3244–3266 (2009).
[194] G. He, J. Bhawalkar, C. Zhao, and P. Prasad, IEEE J. Quantum Electron. **32**, 749–755 (1996).
[195] G. S. He, J. D. Bhawalkar, C. F. Zhao, C. K. Park, and P. N. Prasad, Opt. Lett. **20**, 2393–2395 (1995).
[196] E. V. Chelnokov, N. Bityurin, I. Ozerov, and W. Marine, Appl. Phys. Lett. **89**, 171119 (2006).
[197] G. S. He, L. S. Tan, Q. Zheng, and P. N. Prasad, Chem. Rev. **108**, 1245–1330 (2008).
[198] F. Terenziani, C. Katan, E. Badaeva, S. Tretiak, and M. Blanchard-Desce, Adv. Mater. **20**, 4641–4678 (2008).
[199] F. Scotognella, D. P. Puzzo, M. Zavelani-Rossi, J. Clark, M. Sebastian, G. A. Ozin, and G. Lanzani, Chem. Mater. **23**, 805–809 (2011).
[200] C. Reese and Z. Bao, Adv. Mater. **19**, 4535–4538 (2007).
[201] H. H. Hu, D. A. Fishman, A. O. Gerasov, O. V. Przhonska, S. Webster, L. A. Padilha, D. Peceli, M. Shandura, Y. P. Kovtun, A. D. Kachkovski, I. H. Nayyar, A. E. Masunov, P. Tongwa, T. V. Timofeeva, D. J. Hagan, and E. W. Van Stryland, J Phys. Chem. Lett. **3**, 1222–1228 (2012).
[202] A. E. Siegman, Lasers, (University Science Books, Sausalito, CA 1986), Chap. 14, p. 558.
[203] O. Svelto, Principles of lasers, (Springer, 2010), Chap. 5, p. 163.
[204] R. C. Polson, G. Levina, and Z. V. Vardeny, Appl. Phys. Lett. **76**, 3858–3860 (2000).
[205] T. Yamao, K. Yamamoto, T. Miki, H. Akagami, Y. Nishimoto, and S. Hotta, "Polarized laser oscillation from polygon crystals of thiophene/phenylene co-oligomers grown by liquid-phase growth", presented at 34th International Symposium on Compound Semiconductors, Kyoto, JAPAN, Oct 15–18, 2007.
[206] H. Mizuno, H. Yanagi, F. Sasaki, and S. Hotta, Phys. Status Solidi A **209**, 2437–2440 (2012).
[207] L. He, Ş. K. Özdemir, and L. Yang, Laser Photon. Rev. **7**, 60–82 (2013).
[208] D. J. Gargas, M. C. Moore, A. Ni, S.-W. Chang, Z. Zhang, S.-L. Chuang, and P. Yang, Acs Nano **4**, 3270–3276 (2010).
[209] S. Fujiwara, K. Bando, Y. Masumoto, F. Sasaki, S. Kobayashi, S. Haraichi, and S. Hotta, Appl. Phys. Lett. **91**, 021104 (2007).
[210] H. H. Fang, R. Ding, S. Y. Lu, Y. D. Yang, Q. D. Chen, J. Feng, Y. Z. Huang, and H. B. Sun, Laser Photon. Rev. **7**, 281–288 (2013).
[211] C. Karnutsch, C. Pflumm, G. Heliotis, J. C. Demello, D. D. C. Bradley, J. Wang, T. Weimann, V. Haug, C. Gartner, and U. Lemmer, Appl. Phys. Lett. **90**, 131104 (2007).
[212] E. B. Namdas, M. Tong, P. Ledochowitsch, S. R. Mednick, J. D. Yuen, D. Moses, and A. J. Heeger, Adv. Mater. **21**, 799–802 (2009).
[213] H. Kogelnik and C. Shank, J. Appl. Phys. **43**, 2327–2335 (1972).

[214] K. Yamashita, M. Arimatsu, M. Takayama, K. Oe, and H. Yanagi, Appl. Phys. Lett. **92**, 243306 (2008).
[215] R. Ding, H. H. Fang, Y. Wang, S. Y. Lu, X. L. Zhang, L. Wang, J. Feng, Q. D. Chen, and H. B. Sun, Org. Electron. **13**, 1602–1605 (2012).
[216] H.-H. Fang, R. Ding, S.-Y. Lu, X.-L. Zhang, J. Feng, and H. Sun, J. Mater. Chem. **22**, 24139–24144 (2012).
[217] H.-H. Fang, S.-Y. Lu, X.-P. Zhan, J. Feng, Q.-D. Chen, H.-Y. Wang, X.-Y. Liu, and H.-B. Sun, Org. Electron. **14**, 762–767 (2013).
[218] S. Kena-Cohen, M. Davanco, and S. R. Forrest, Phys. Rev. Lett. **101**, 116401 (2008).
[219] C. Schneider, A. Rahimi-Iman, N. Y. Kim, J. Fischer, I. G. Savenko, M. Amthor, M. Lermer, A. Wolf, L. Worschech, and V. D. Kulakovskii, Nature **497**, 348–352 (2013).
[220] S. Christopoulos, G. B. H. von Högersthal, A. J. D. Grundy, P. G. Lagoudakis, A. V. Kavokin, J. J. Baumberg, G. Christmann, R. Butté, E. Feltin, J. F. Carlin, and N. Grandjean, Phys. Rev. Lett. **98**, 126405 (2007).
[221] D. Bajoni, J. Phys. D **45**, 313001 (2012).
[222] L. V. Butov, Nature **447**, 540–541 (2007).
[223] H. Deng, G. Weihs, D. Snoke, J. Bloch, and Y. Yamamoto, Proc. Natl. Acad. Sci. **100**, 15318–15323 (2003).
[224] A. Das, J. Heo, M. Jankowski, W. Guo, L. Zhang, H. Deng, and P. Bhattacharya, Phys. Rev. Lett. **107**, 066405 (2011).
[225] S. Kena-Cohen and S. R. Forrest, Nat. Photonics **4**, and371–375 (2010).
[226] A. Kavokin, Nat. Photonics **7**, 591–592 (2013).
[227] P. Bhattacharya, B. Xiao, A. Das, S. Bhowmick, and J. Heo, Phys. Rev. Lett. **110**, 206403 (2013).
[228] P. Del Carro, A. Camposeo, L. Persano, S. Tavazzi, M. Campione, A. Papagni, L. Raimondo, L. Silvestri, P. Spearman, R. Cingolani, and D. Pisignano, Appl. Phys. Lett. **92**, 063301 (2008).
[229] K. Bando, T. Takano, H. Fujii, T. Nakano, D. Makino, S. Kumeta, F. Sasaki, and S. Hotta, Appl. Phys. Lett. **103**, 023304 (2013).
[230] C. Simbrunner, G. Hernandez-Sosa, F. Quochi, G. N. Schwabegger, C. Botta, M. Oehzelt, I. Salzmann, T. Djuric, A. Neuhold, and R. Resel, Acs Nano **6**, 4629–4638 (2012).
[231] K. Takazawa, J.-I. Inoue, and K. Mitsuishi, ACS Appl. Mater. Inter. **5**, 6182–6188 (2013).
[232] F. Quochi, F. Cordella, A. Mura, G. Bongiovanni, F. Balzer, and H. G. Rubahn, J. Phys. Chem. B **109**, 21690–21693 (2005).
[233] Y. S. Zhao, A. D. Peng, H. B. Fu, Y. Ma, and J. N. Yao, Adv. Mater. **20**, 1661–1665 (2008).
[234] S. M. Yoon, J. Lee, J. H. Je, H. C. Choi, and M. Yoon, ACS Nano. **5**, 2923–2929 (2011).
[235] Y. L. Yan and Y. S. Zhao, Adv. Funct. Mater. **22**, 1330–1332 (2012).
[236] K. Takazawa, J.-I. Inoue, K. Mitsuishi, and T. Takamasu, Phys. Rev. Lett. **105**, 67401 (2010).
[237] M. C. A. Bernanose and P. Vouaux, J. Chim. Phys. **50**, 64–68 (1953).
[238] M. Pope, H. Kallmann, and P. Magnante, Chem. Phys. **38**, 2042–2043 (1963).
[239] C. E. Swenberg and M. Pope, Electronic processes in organic crystals and polymers, (Oxford University Press, Oxford, 1999).
[240] C. W. Tang and S. A. VanSlyke, Appl. Phys. Lett. **51**, 913–915 (1987).
[241] J. Burroughes, D. Bradley, A. Brown, R. Marks, K. Mackay, R. Friend, P. Burns, and A. Holmes, Nature **347**, 539–541 (1990).
[242] P. Andrew, G. A. Turnbull, I. D. Samuel, and W. L. Barnes, Appl. Phys. Lett. **81**, 954–956 (2002).
[243] T. Rabe, P. Görrn, M. Lehnhardt, M. Tilgner, T. Riedl, and W. Kowalsky, Phys. Rev. Lett. **102**, 137401 (2009).
[244] S. Hotta, T. Yamao, S. Bisri, T. Takenobu, and Y. Iwasa, J. Mater. Chem. C **2**, 965–980 (2014).
[245] M. Muccini, W. Koopman, and S. Toffanin, Laser Photon. Rev. **6**, 258–275 (2012).
[246] J. Zaumseil, in Organic Electronics: Emerging Concepts and Technologies (Wiley-VCH, 2013), pp. 187–213.
[247] F. Cicoira and C. Santato, Adv. Funct. Mater. **17**, 3421–3434 (2007).
[248] R. Capelli, S. Toffanin, G. Generali, H. Usta, A. Facchetti, and M. Muccini, Nat. Mater. **9**, 496–503 (2010).
[249] J. Kalinowski, J. Phys. D: Appl. Phys. **32**, R179 (1999).
[250] H. Nakanotani, M. Saito, H. Nakamura, and C. Adachi, Appl. Phys. Lett. **95**, 103307 (2009).
[251] S. Z. Bisri, T. Takenobu, K. Sawabe, S. Tsuda, Y. Yomogida, T. Yamao, S. Hotta, C. Adachi, and Y. Iwasa, Adv. Mater. **23**, 2753–2758 (2011).
[252] M. Melucci, L. Favaretto, M. Zambianchi, M. Durso, M. Gazzano, R. Capelli, M. Muccini, V. Biondo, S. Toffanin, and S. Troisi, Chem. Mater. **25**, 668–676 (2013).
[253] M. Muccini, Nat. Mater. **5**, 605–613 (2006).
[254] H. Yersin, in Transition Metal and Rare Earth Compounds (Springer, 2004), pp. 1–26.
[255] K. Sawabe, M. Imakawa, M. Nakano, T. Yamao, S. Hotta, Y. Iwasa, and T. Takenobu, Adv. Mater. **24**, 6141–6146 (2012).
[256] X. J. Li, Y. X. Xu, F. Li, and Y. G. Ma, Org. Electron. **13**, 762–766 (2012).
[257] J. Cornil, J. L. Brédas, J. Zaumseil, and H. Sirringhaus, Adv. Mater. **19**, 1791–1799 (2007).
[258] P. Levesque, C. Aguirre, M. Paillet, F. Lapointe, B. St-Antoine, P. Desjardins, and R. Martel, Adv. Mater. **21**, 3087–3091 (2009).
[259] M. Liu, X. Jiang, S. Liu, P. Herguth, and A. Jen, Macromolecules **35**, 3532–3538 (2002).
[260] L.-L. Chua, J. Zaumseil, J.-F. Chang, E. Ou, P. Ho, H. Sirringhaus, and R. Friend, Nature **434**, 194–199 (2005).
[261] I. Hulea, S. Fratini, H. Xie, C. Mulder, N. Iossad, G. Rastelli, S. Ciuchi, and A. Morpurgo, Nat. Mater. **5**, 982–986 (2006).
[262] T. Takahashi, T. Takenobu, J. Takeya, and Y. Iwasa, Adv. Funct. Mater. **17**, 1623–1628 (2007).
[263] M. Lehnhardt, T. Riedl, T. Weimann, and W. Kowalsky, Phys. Rev. B **81**, 165206 (2010).
[264] H.-H. Fang, Q.-D. Chen, R. Ding, J. Yang, Y.-G. Ma, H.-Y. Wang, B.-R. Gao, J. Feng, and H.-B. Sun, Opt. Lett. **35**, 2561–2563 (2010).
[265] C. Lee, K. Wong, J. Huang, S. Frolov, and Z. Vardeny, Chem. Phys. Lett. **314**, 564–569 (1999).
[266] H. Yersin, A. F. Rausch, R. Czerwieniec, T. Hofbeck, and T. Fischer, Coord. Chem. Rev. **255**, 2622–2652 (2011).

[267] H. Yersin, Top Curr. Chem. **241**, 1–26 (2004).
[268] H. Yersin and J. Strasser, Coord. Chem. Rev. **208**, 331–364 (2000).
[269] F. Cordella, F. Quochi, M. Saba, A. Andreev, H. Sitter, N. S. Sariciftci, A. Mura, and G. Bongiovanni, Adv. Mater. **19**, 2252–2256 (2007).
[270] M. M. Mróz, G. Sforazzini, Y. Zhong, K. S. Wong, H. L. Anderson, G. Lanzani, and J. Cabanillas-Gonzalez, Adv. Mater. **25**, 4347–4351 (2013).
[271] M. Lehnhardt, T. Riedl, U. Scherf, T. Rabe, and W. Kowalsky, Org. Electron. **12**, 1346–1351 (2011).
[272] S. Schols, L. Van Willigenburg, S. Steudel, J. Genoe, and P. Heremans, IEEE J. Quantum Electron. **46**, 62–67 (2010).
[273] X. Xing, T. Tsuboi, Y. Nakai, F. Wang, B. Qi, Z. Chen, B. Qu, L. Xiao, and Q. Gong, Org. Electron. **13**, 195–198 (2012).
[274] J. Li, S. Takaishi, N. Fujinuma, K. Endo, M. Yamashita, H. Matsuzaki, H. Okamoto, K. Sawabe, T. Takenobu, and Y. Iwasa, J. Mater. Chem. **21**, 17662–17666 (2011).
[275] K. Kajiwara, K. Terasaki, T. Yamao, and S. Hotta, Adv. Funct. Mater. **21**, 2854–2860 (2011).
[276] T. Yamao, Y. Shimizu, K. Terasaki, and S. Hotta, Adv. Mater. **20**, 4109–4112 (2008).
[277] M. C. Gwinner, S. Khodabakhsh, M. H. Song, H. Schweizer, H. Giessen, and H. Sirringhaus, Adv. Funct. Mater. **19**, 1360–1370 (2009).
[278] T. Yamao, Y. Sakurai, K. Terasaki, Y. Shimizu, H. Jinnai, and S. Hotta, Adv. Mater. **22**, 3708–3712 (2010).
[279] A. Okada, Y. Makino, S. Hotta, and T. Yamao, Phys. Status Solidi C **9**, 2545–2548 (2012).
[280] S. Z. Bisri, K. Sawabe, M. Imakawa, K. Maruyama, T. Yamao, S. Hotta, Y. Iwasa, and T. Takenobu, Sci. Rep. **2**, 985 (2012).
[281] H. Nakanotani, M. Saito, H. Nakamura, and C. Adachi, Adv. Funct. Mater. **20**, 1610–1615 (2010).
[282] H. Nakanotani and C. Adachi, Adv. Opt. Mater. **1**, 422–427 (2013).
[283] S. Richardson, O. Gaudin, G. Turnbull, and I. Samuel, Appl. Phys. Lett. **91**, 261104 (2007).